to be submitted to Astrophys. J.

Numerical Study on the Rotational Collapse of Strongly Magnetized Cores of Massive Stars

Shoichi Yamada and Hidetomo Sawai

Science & Engineering, Waseda University, 3-4-1 Okubo, Shinjuku, Tokyo 169-8555

ABSTRACT

Hydrodynamics of the rotational collapse of strongly magnetized massive stellar cores has been studied numerically. Employing a simplified microphysics and 2D non-relativistic MHD code, we have done a parametric research with respective to the strength of magnetic field and rotation, and have paid particular attention to the systematics of dynamics. It is assumed initially that the rotation is almost uniform and the magnetic field is constant in space and parallel to the rotation axis. We have found that the combination of rotation and magnetic field can lead to a jet-like prompt explosion in the direction of the rotational axis, which would not be produced by either of them alone. Although the results appear to be consistent with those by LeBlanc & Wilson and Symbalisty, the magnetic fields behind the shock wave, not in the inner core, is the main driving factor of the jet. The fields are amplified by the strong differential rotations in the outer core between the shock wave and the boundary of the inner and outer cores, enhanced further by the lateral matter motions induced either by an oblique shock wave (for a strong shock case) or possibly by the MRI(magneto-rotational instability)-like instability (for a weak shock case). We have also calculated the gravitational wave forms in the quadrupole approximation. Although the wave form from a non-rotating magnetic core is qualitatively different from those from rotating cores, the amplitude is about an order of magnitude smaller. Otherwise we have found no substantial difference in the first burst of gravitational waves among the magnetized and non-magnetized models, since the bounce is mainly driven by the combination of the matter pressure and the centrifugal force.

Subject headings: supernovae: collapse, rotation—magnetars: pulsar, magnetic field

1. Introduction

Numerical studies of rotational collapse of massive stellar cores in the context of collapse-driven supernovae date back to the pioneering paper by LeBlanc and Wilson (1970). Since this is much earlier than the discovery of the weak neutral current, the scenario and micro physics they adopted are obsolete by today's standard. However, their conclusion seems to be widely accepted as generically correct : the jet-like explosion is induced if there is a suitable combination of rapid rotation and strong magnetic field. Since then, not many papers have been dedicated to this theme (Meier et al. 1976; Bisnovatyi-Kogan et al. 1976; Ardeljan 1979; Müllrer and Hillebrandt 1979; Ohnishi 1983; Symbalisty 1984; Ardeljan 2000). Most serious among them is the paper by Symbalisty (1984). He performed a couple of 2D MHD simulations of both rotational and magneto-rotational collapses of a realistic iron core of a $15M_{\odot}$ evolved star. He also found a strong jet-like anisotropic explosion for the combination of very strong magnetic field and very rapid rotation.

Symbalisty's models explain why so little attention has been paid to this subject. In his models, the magnetic field was assumed to be very large $\sim 10^{13}$G from the outset. The maximum field strength at the end of simulations was as great as $\sim 10^{16}$G. This is about three orders of magnitude larger than the typical field strength on the pulsar surface. This is not surprising, though. If the magnetic fields were to have a significant influence on the dynamics of the core in the dynamical time scale, the magnetic stress should be comparable to the matter pressure. This simply corresponds to the field strength seen in the Symbalisty's models. Most researchers thought that this large magnetic field is unrealistic and regarded these works as of academic interest.

This may be changing these days, since it is suggested observationally that some pulsars are indeed very strongly magnetized. Anomalous X-ray pulsars and soft gamma-ray repeaters are believed to be such objects (Thompson and Duncan 1996; Zhang and Harding 2000; Guseinov et al. 2003). Their magnetic fields are inferred from the spin down rates with an assumption that the magnetic dipole radiation is responsible for the deceleration. The large X-ray luminosity of anomalous X-ray pulsars cannot be accounted for by the loss of rotation energy and is supposed to be supplied by the dissipation of the magnetic fields of the strength quoted above (Thompson and Duncan 1996). They are collectively referred to as "magnetar". There are about ten of them discovered so far. They are supposed to make a distinct group from the ordinary radio pulsars (Zhang and Harding 2000; Guseinov et al. 2003). In fact, the lower end of the magnetar and the higher end of the ordinary radio pulsar have a similar strength of magnetic field but have quite different X-ray activities. Although the magnetar may be a minor subgroup of neutron stars, their origin and formation should be clarified.

It has been pointed out lately that the collapse-driven supernovae might be generically asymmetric (Wang et al. 1996; Leonard et al. 2000; Wheeler et al. 2000). Although still controversial, polarimetric observations suggest that the anisotropically expanding envelope has commonly an aspect ratio of about two if the polarization originates from the asymmetry of scattering envelope. SN1987A is one of such globally asymmetric explosions (Wang et al. 2002). Although it is supposed that the rapid rotation of progenitors is the most promising explanation for the asymmetry, we do not know exactly how (Chevalier et al. 1989; Ishikawa et al. 1992; Khokhlov et al. 1999; Shimizu et al. 1994). It is widely accepted that highly collimated jets are involved in gamma ray bursts (GRB). One of the most promising scenarios of GRB is the so-called "collapsar" model (Woosley 1993; MacFadyen 1999). The rotational collapse of massive stars and subsequent black hole formation is invoked in this model. It is noted that the so-called "hypernovae", which have broad line features in the spectra and hence are supposed to have very high expansion velocities, are believed to be highly asymmetric supernovae. Some of them may be associated with GRB (Wheeler et al. 2000; Stanek et al. 2003). Although MacFadyen (1999) demonstrated that the GRB jet formation does not necessarily require magnetic fields, it may be possible that strong magnetic fields play an important role in the central engine of this very energetic phenomenon. Hence the numerical study of magneto-rotational collapse will be important for the systematic and unified understanding of the fate of massive stars (Heger et al. 2003).

It should be noted here that the currently favored paradigm for the collapse-driven supernova is a so-called 'neutrino-heating mechanism'. According to many simulations, the shock wave generated by the core bounce stalls inside the core and the so-called prompt explosion fails. In the neutrino-heating scenario, it is supposed that neutrinos diffusing out of the prot-neutron star heat matter behind the stagnated shock wave and induce explosion in the longer time scale than the prompt explosion. Recent state-of-the-art simulations (Liebendörfer et al. 2001; Rampp and Janka 2000; Thompson et al. 2003), however, have not succeeded in producing explosions. Something is still critically missing. Although we do not intend to claim in this paper that the magnetic fields are the missing piece, we should leave no stones unturned. Since the numerical investigations of magneto-rotational collapse of massive stellar cores have been so far very sporadic in the context of supernovae, we focus in this paper on the parametric research of the systematics of dynamics, and as a first step we start with the prompt explosion. For that purpose the electron captures, complicated nuclear equation of state (EOS) and the neutrino transport have been replaced by the phenomenological parametric EOS which was used by Yamada and Sato (1994). This is an extension of the paper by Yamada and Sato (1994) in which the effect of rotation on the prompt explosion was investigated using the same method. This method is useful to elucidate the trend of dynamics when the strength of rotation and/or magnetic field is

changed, and plays a complementary role to more realistic simulations. We have assumed very strong magnetic fields at the beginning of collapse and it is beyond the scope of this paper to address the origin of such a large magnetic field prior to the collapse (Spruit 2002; Heger et al. 2003). This is just the first step of our project to study issues of relevance for magnetized supernovae.

This paper is organized as follows. In the next section, we describe the numerical method and the assumptions concerning microphysics, initial magnetic fields and angular momentum distributions. In section 3, we show the numerical results of dynamics as well as the time evolutions of the angular momentum distributions and the magnetic fields. Wave forms of gravitational radiation emitted around the core bounce are also presented. In section 4 we give some discussions and conclude the paper.

2. Models and Numerical Methods

2.1. Models

We have done two dimensional MHD simulations with axisymmetric geometry. The spherically symmetric density profile of the central $1.4M_\odot$ of a realistic $15M_\odot$ model by Woosley (1995) has been employed, and rotation and magnetic field are just added. Hence the initial models are not in equilibrium. The shellular rotation is assumed with the angular velocity distribution

$$\Omega(r) \;=\; \Omega_0 \, \frac{r^2}{r^2 + R^2} \quad , \tag{1}$$

where Ω_0 and R are constants. R is set to be 1.0×10^8cm for all the models so that the rotation is essentially uniform except for the outermost part of the core. It is known that the rotation tends to become cylindrical later on regardless of the initial rotation (Janka et al. 1989; Yamada and Sato 1994). The initial magnetic fields are assumed to be uniform and parallel to the rotational axis. The strengths of rotation and magnetic field are summarized in Table 1 for all the models together with other model parameters. It should be noted that the latest theoretical study by Heger et al. (2003) predicts that the progenitor is likely to be a slow rotator and to have a weak magnetic field prior to the collapse. Although this is a very important result, the precollapse evolutions of rotation and magnetic fields have still uncertainties and the result will be subject to change. Hence we prefer here to have the initial rotation and magnetic field as model parameters and vary arbitrarily.

2.2. Numerical Code

The MHD equations in the following form has been finite-differenced on the spherical coordinates:

$$\frac{D\rho}{Dt} = -\rho\nabla\cdot\boldsymbol{v}, \tag{2}$$

$$\rho\frac{D\boldsymbol{v}}{Dt} = -\nabla p - \rho\nabla\Phi + \frac{1}{4\pi}(\nabla\times\boldsymbol{B})\times\boldsymbol{B}, \tag{3}$$

$$\rho\frac{D}{Dt}\left(\frac{e}{\rho}\right) = -p\nabla\cdot\boldsymbol{v}, \tag{4}$$

$$\frac{\partial\boldsymbol{B}}{\partial t} = \nabla\times(\boldsymbol{v}\times\boldsymbol{B}), \tag{5}$$

where ρ, $\boldsymbol{v}$, e, $\boldsymbol{B}$, Φ are density, velocity, internal energy density, magnetic field and gravitational potential, respectively. The Lagrangian derivative is denoted as D/Dt. The magnetic permeability is assumed to be unity in the following simulations. The ZEUS-2D code developed by Stone and Norman (1992) has been used with a modification of EOS as explained below. We do not describe the details of the code here and refer the readers to the original papers (Stone and Norman 1992). Instead we give some important feature of the code. The code solves the induction equation as shown in Eq. (5). In so doing the so-called constrained transport (CT) method is adopted to ensure the divergence-free of numerical solutions. Furthermore, the method of characteristics (MOC) is implemented to properly handle Alfvén waves. Shock waves are captured by the artificial viscosity of von Neuman-Richtmyer type. In this paper, the second order accurate interpolation in space is chosen. The operator splitting and the predictor and corrector type integration are utilized for the time integration of the energy equation. The gravitational potential is obtained by solving a Poisson equation with the ICCG (Incomplete Cholesky Conjugate Gradient) method.

The spherical mesh with $300(r)\times30(\theta)$ grid points is used for all the computations. The equatorial symmetry is assumed. The radial grid is non-uniform extending to $\sim$ 2000km with finer zones near the center while the polar grid is uniform. The grid is fixed in time except for a rezoning to a more centrally-concentrated grid when the central density reaches $\sim 10^{12}\mathrm{g/cm}^3$. About 10^5 time steps are computed for each model. The typical error in the total energy is about a few times 10^{50} ergs.

2.3. EOS

This paper is not intended to do realistic simulations and address the supernova mechanism but to do some numerical experiments and grasp the systematics of hydrodynamics

with rapid rotation and strong magnetic field. For this purpose, we simplify other physics drastically. This is done by employing the parametric EOS which was formerly used by Yamada and Sato (1994) to investigate the systematics of rotational collapse of stellar cores. This was designed to mimic electron captures on nuclei and nucleons, neutrino trapping and shock weakening due to neutrino losses and iron dissociations, and thus spares us the explicit treatment of them. It also allows us to produce artificially both successful and failed prompt explosions. This in turn enables us to demonstrate clearly whether the rotation and/or magnetic field help explosion or not.

The EOS consists of two parts, the cold part and the thermal part:

$$p_{tot}(\rho, \varepsilon_t) \;=\; p_c(\rho) \;+\; p_t(\rho, \varepsilon_t). \tag{6}$$

The former roughly corresponds to the pressures of degenerate electrons and neutrinos and is of the polytropic form with a variable adiabatic index according to the density regimes:

$$p_c(\rho) \;=\; K\rho^{\Gamma} \quad , \tag{7}$$

which is also shown in Fig. 1. The boundary of regimes I and II corresponds to the onset of electron capture and is set to be 10^9g/cm^3. The adiabatic index in the density regime I is 4/3 while in the density regime II it is slightly lower than 4/3 due to the electron capture on nuclei and nucleons. The value is obtained from the remaining lepton fraction at rho_2 as

$$\left[\frac{Y_l(\rho_2)}{Y_l(\rho_1)}\right]^{4/3} \;=\; \frac{p_2}{p_1} \;=\; \left[\frac{\rho_2}{\rho_1}\right]^{\Gamma_2 - 4/3} \quad . \tag{8}$$

At density ρ_2 ($= 10^{12}$g/cm^3), neutrinos are assumed to be trapped and in β-equilibrium. The adiabatic index recovers to 4/3 in the density regime III in which the lepton fraction becomes unchanged. The regime IV corresponds to the super-nuclear density, where the matter becomes very stiff due mainly to the repulsive nuclear forces. The transition density is $\rho_3 = 2.8 \times 10^{14}$g/cm^3 and the adiabatic index is assumed to be 2.5 above ρ_3.

The thermal part of the pressure, which originates from the thermal energy generated by the shock dissipation, is assumed to take the following form:

$$p_t(\rho, \varepsilon_t) \;=\; (\gamma_t \,-\, 1)\,\rho\,\varepsilon_t \quad , \tag{9}$$

where we refer to γ_t as the thermal stiffness. It stands for the reduction of the pressure by the dissociation of irons to α particles and nucleons as well as the neutrino cooling.

We know that larger values of adiabatic index in the regime II and/or of the thermal stiffness are favorable for successful prompt explosions. In this paper, we fix the thermal

stiffness to 1.3 and adopt two values, 1.31 and 1.29, for the adiabatic index in the regime II, which correspond to the trapped lepton fractions, 0.38 and 0.35. As we will show later, the former case gives a successful prompt explosion, while the latter does not. We will then look into the difference the rotation and/or magnetic field make to them.

2.4. Gravitational Wave

We are also interested in the gravitational waves generated as a burst mainly around the core bounce. Following the common practice we employ the quadrupole approximation for the evaluation of wave forms based on the results of Newtonian simulations (Yamada and Sato 1995; Zwerger et al. 1997). The major change is the inclusion of the magnetic field contribution to the mass quadrupole. Hence the wave form is given as

$$h^{TT}_{\theta\theta} = -h^{TT}_{\phi\phi} = \frac{1}{8}\sqrt{\frac{15}{8}}\,\sin^2\theta\,\frac{d^2}{dt^2}M^{E2}_{20}\,/\,D \quad , \tag{10}$$

$$M^{E2}_{20} \equiv \frac{G}{c^4}\frac{32\,\pi^{3/2}}{\sqrt{15}}\int_0^1\int_0^\infty \rho_{tot}\left(\frac{3}{2}\,\mu^2 - \frac{1}{2}\right) r^4 dr\,d\mu \quad , \tag{11}$$

$$\rho_{tot} = \rho + \frac{1}{8\pi c^2}B^2 \quad , \tag{12}$$

where h is the metric perturbation, c, G are the light velocity and gravitational constant, respectively, and D is the distance to the observer. The superscript, "TT", stands for the transverse traceless part and the subscripts, "$\theta\theta$" and "$\phi\phi$", specify two polarization states of the gravitational wave. The total mass quadrupole is denoted as M^{E2}_{20}, and the total density, ρ_{tot}, is the sum of the matter and magnetic field contributions. In the above equations, we have employed the axisymmetry of the system and the cosine of the polar angle is designated as μ. Since this formula includes a second time derivative, it is not suitable for numerical evaluations. We use the MHD equations, Eqs.(2)$\sim$(5), to replace the time derivative by space derivatives which are easier to handle numerically. This is also the well known procedure which was also taken in our previous paper on the rotational collapse (Blanchet et al. 1990; Finn and Evans 1990; Mönchmeyer et al. 1991; Yamada and Sato 1995). Although it is possible to eliminate all the time derivatives this way, it would make the formulae quite complicated and numerical evaluations formidable again. Hence we prefer in this paper to leave the first time derivatives as

$$\frac{d^2}{dt^2}M^{E2}_{20} = \frac{G}{c^4}\frac{32\,\pi^{3/2}}{\sqrt{15}}\int_0^1 d\mu\int_0^\infty dr\left\{\rho\,r^2\left[v_r^2(3\mu^2-1) + v_\theta^2(2-3\mu^2) - v_\phi^2 - 6v_r v_\theta\,\mu\sqrt{1-\mu^2} - r\,\frac{\partial\Phi}{\partial r}(3\mu^2-1) + \frac{\partial\Phi}{\partial\theta}\,\mu\sqrt{1-\mu^2}\right]\right.$$

$$
\begin{aligned}
&- \; r^3 \left[q_r(3\mu^2-1) \; - \; 3q_\theta \, \mu \sqrt{1-\mu^2} \right] \\
&+ \; r^3 \left[(3\mu^2-1) \, \frac{1}{c} \, (\boldsymbol{j} \times \boldsymbol{B})_r \; - \; 3\mu \sqrt{1-\mu^2} \, \frac{1}{c} \, (\boldsymbol{j} \times \boldsymbol{B})_\theta \right] \\
&+ \; \frac{1}{8\pi c} \frac{d}{dt} \left[\frac{\partial}{\partial \theta} \left[B_r r^3 (3\mu^2-1) \right] E_\phi \; - \; \frac{\partial}{\partial r} \left[B_\theta \, r^3 (3\mu^2-1) \right] r E_\phi \right. \\
&\qquad\qquad + \; \frac{\partial}{\partial r} \left[B_\phi \, r^3 (3\mu^2-1) \right] r E_\theta \\
&\qquad\qquad \left. - \; \frac{1}{\sin\theta} \frac{\partial}{\partial \theta} \left[B_\phi \sin\theta \, r^3 (3\mu^2-1) \right] E_r \right] \Bigg\} , \qquad (13)
\end{aligned}
$$

where B_r, B_θ, B_ϕ are the r-, θ-, ϕ-components of magnetic field and E_r, E_θ, E_ϕ are the electric field ($\boldsymbol{E} = -c\boldsymbol{v} \times \boldsymbol{B}$) counter part. The time derivatives are calculated from the numerical data at three successive time steps. Although the wave forms thus obtained are a little noisy in short time scales as seen in section 3.3, the overall feature is well reproduced.

3. Results

We show the numerical results of 2D MHD simulations here. The dynamics, the field amplification with the angular momentum transfer, and the gravitational wave forms are presented separately in detail.

3.1. dynamics

We begin with the spherically symmetric reference models. Models MS1 and MF1 differ in the lepton fraction at the neutrino trapping (see Eq. (8)). The difference is reflected in Γ_2. As explained in §2.3, we can obtain both a successful prompt explosion, MS1, and a failed one, MF1, by varying this parameter. A larger Y_l or a larger Γ_2 is favorable for explosion (Takahara and Sato 1984; Yamada and Sato 1994), since it gives a larger inner core and, as a result, a smaller outer core, thus reducing the burden for the shock wave. Here we define the inner core as the part of the core inside the sonic point at which the infall velocity equals to the local sound velocity. The rest of the core is referred to as the outer core. In Model MS1 we have an inner core of $0.84 M_\odot$ at the bounce, which is defined to be the time of the first emergence of positive velocity at the center. The maximum central density is $4.6 \times 10^{14} \mathrm{g/cm^3}$. The strong prompt shock wave reaches the core surface ($r \sim 1.5 \times 10^8 \mathrm{cm}$) unstalled with the explosion energy of $2.2 \times 10^{51} \mathrm{erg}$ and the ejected mass of $0.42 M_\odot$. Here the explosion energy and the ejected mass are defined as the sum of the total energy (the

sum of the kinetic, internal and gravitational energies) and the mass, respectively, over the fluid elements with the positive total energy and radial velocity at the end of computations. It should be noted that this is a very crude estimate of the true explosion energy. We use this quantity just as a measure of the strength of explosion for comparison among various models. On the other hand, Model MF1 with $Y_l = 0.35$ fails to explode in the prompt way. The inner core mass is $0.78 M_\odot$ at the core bounce. The central density reaches $4.9 \times 10^{14} \mathrm{g/cm^3}$ at maximum. There is no fluid element with the positive total energy at the end of the simulation. The shock propagations for these two models are shown in Fig. 2.

Models MS2 and MF2 are rotation-only cases. The ratio of the rotational energy to the gravitational energy, $|T/W|$, is assumed to be 1.5% at the beginning of computations for these models. It should be noted that this is a very rapid rotation. This corresponds to $\Omega_0 = 6.8 \mathrm{s^{-1}}$. It is well known observationally that O, B stars, typical progenitors of collapse-driven supernovae, have surface rotation velocities of about 200km/s on the main sequence (Tassoul 1978). Those stars may form a rotating core with $|T/W| \lesssim 1\%$ prior to the collapse if the magnetic field does not exist in the progenitor star, and this value is already large enough to account for pulsar rotations (Woosley and Heger 2003). If, on the other hand, the magnetic field does exist in the progenitor and is amplified somehow in the evolution, the value of $|T/W|$ might be smaller by orders of magnitude (Heger et al. 2003). Since we do not know at present what the initial rotation velocity is, here we take an extreme value to see clearly the effect of rotation on dynamics. In Model MS2, the core bounce occurs when the central density reaches $1.1 \times 10^{13} \mathrm{g/cm^3}$, much lower than the spherical model MS1. This is simply due to the centrifugal forces which tend to stabilize the core against collapse (Shapiro and Teukolsky 1983; Mönchmeyer and Müller 1989). As shown in Fig. 3, the inner core becomes oblate at the bounce. It is slightly larger, $0.90 M_\odot$, than the spherical model MS1 at the core bounce. Although this should be a little bit more advantageous for the prompt explosion, the outcome is a failed explosion. This is because the centrifugal force prevents the core from shrinking sufficiently to launch a strong shock wave. Since we assumed a rather large thermal stiffness ($\gamma_T \sim 1.3$), the shock wave continues to expand and becomes prolate as seen in Fig. 3 with a tiny amount of matter ($6 \times 10^{-3} M_\odot$ with 2.6×10^{49}erg) emitted in the direction of the rotation axis. This demonstrates clearly that the rapid rotation is harmful for the prompt explosion (Mönchmeyer and Müller 1989; Yamada and Sato 1994) and is nothing but a reconfirmation of the previous results by Yamada and Sato (1994). Model MF2 does not differ from MS2 qualitatively. The oblate inner core ($0.71 M_\odot$) bounces with a maximum central density of $3.9 \times 10^{13} \mathrm{g/cm^3}$. Again the prompt shock wave is weakened rapidly after the launch and we find essentially no explosion at the end. This again indicates that the rotation is not of any help for the prompt explosion which already fails for the spherical model MF1.

Let us now turn to the models with non-vanishing magnetic fields. We take Model MS4 as the reference case. The time evolutions are presented in Figs. 4 to 6, in which velocity fields and poloidal magnetic field lines are superimposed on the density color contours. Fig. 4 corresponds to the bounce. The flattened inner core of $0.9M_\odot$ bounces with a maximum central density of 1.2×10^{13}g/cm^3. The fast magnetohydrodynamic shock wave is launched in the direction of the rotation axis. Fig. 5 clearly shows that the flows start to converge to the axis, forming a jet. The shock wave becomes prolate with an aspect ration of about 1.7. As seen in Fig. 6, we have a successful but somewhat weak prompt explosion. Note again that the model with the same rotation but without magnetic fields (Model MS2) fails to explode. The explosion energy is 3.8×10^{50}erg and the ejected mass is $0.06M_\odot$ in this model. Although this is not a strong explosion in terms of the total explosion energy, it should be noted that the isotropic equivalent energy, which is the explosion energy one would obtain if the jet were extending over the whole solid angle, still reaches the canonical explosion energy. The magnetic fields inside the proto neutron star is $\gtrsim 10^{14}$G on average and becomes as large as 3×10^{15}G locally at the end of the simulation. Although this is much larger than the canonical magnetic fields of pulsars, its stress is still smaller than the matter pressure. It is incidentally mentioned that the value is comparable to those found by Symbalisty (1984). The final $|T/W|$ is 7.0% and $|E_m/W|$ is 1.1%. The jet is produced by the toroidal fields behind the shock wave near the rotation axis, which are generated from the initial poloidal fields by strong differential rotations there. In fact, the ratio of the magnetic stress of toroidal fields to the matter pressure becomes greatest in this region (see also the next section). MS3, which has a smaller magnetic field, is qualitatively similar to MS4. The jet-like explosion occurs also in this case with a similar explosion energy (3.2×10^{50}erg) and ejected mass ($0.066M_\odot$). The inner core mass and the maximum density etc. are summarized in Table 2 together with other models.

Now we move on to the models with a smaller $Y_l(= 0.35)$, that is, the MF sequence. Let us repeat that neither the spherical model (MF1) nor the pure rotation model (MF2) obtains a successful explosion in this sequence. Although it is not our intention in this paper to do realistic simulations, we think that this sequence is a little bit closer to the reality than the MS sequence. Let us first look into Model MF3. This is a very rapid rotator with a very strong magnetic field from the beginning like MS4. The dynamics is quite similar to MS4. The flattened core bounces with the inner core of $0.74M_\odot$ like Model MF2 which has the same $|T/W|$ prior to the collapse but has no magnetic fields. The maximum central density (4.2×10^{13}g/cm^3) is also close to that of MF2. A fast magnetohydrodynamic shock is then launched and propagates preferentially in the direction of the rotation axis. The stress of the toroidal magnetic fields generated from the initially poloidal magnetic fields by differential rotations collimates the matter flow into a jet. As shown in Fig. 7, this shock wave reaches the

core surface unstalled and ejects matter of $0.065 M_\odot$ with an explosion energy 3.8×10^{50}erg. It is interesting that the explosion energy is comparable to Models MS3 and MS4 which have a larger trapped lepton fraction. Although MF3 has smaller pressure support from matter, the inner core collapses a bit deeper and, as a result, the stronger differential rotations lead to the larger toroidal magnetic fields just above the inner core surface near the rotation axis, which generate the stronger jet. Farther out, however, the region with strong toroidal fields is narrower and the jet is less collimated. All these effects conspire to eject mass and energy comparable to MS3 and MS4. The aspect ratio of the prolate shock wave itself is again (~ 1.7) in this model.

Models MF4 to MF7 are meant to study the dependence of the above results on the rotation velocity. MF4 is a pure magnetic field model. In accordance with Symbalisty's result (Symbalisty 1984), this model does not lead to an explosion, although a tiny amount of matter is still expanding at the end of the simulation. The inner core becomes slightly oblate at bounce due to the anisotropic stress of poloidal magnetic fields. The central density reaches 4.6×10^{14}g/cm^3. Although the contraction of the core amplifies the magnetic fields frozen in fluid elements, the ratio of the magnetic energy to the gravitational energy, $|E_m/W|$ is much smaller than for MF3, in which magnetic fields are amplified by differential rotations also. The shock wave propagates faster in the direction of the rotation axis also in this case and becomes slightly prolate at first (the left panels of Fig. 8), but it becomes almost spherical at the end (the right panels of Fig. 8). When the rotation of $|T/W| = 0.1\%$ is added (MF5), the dynamics is already changed remarkably. As seen in Fig. 9, the very narrow jet is generated in the same mechanism as explained. An interesting thing is that the amount of ejected matter and its energy are much larger than Model MF3. In fact, matter velocities reach half the light velocity in the jet. Recent stellar evolution models suggest that the initial rotation might be substantially slow if the magnetic torque is taken into account (Heger et al. 2003). Model MF5 suggests that if the magnetic field is very large, the jet-like explosion may be still possible even if the rotation is slow. It is, however, mentioned that this result needs further investigation , since the jet is confined to the vicinity of the rotation axis and our simulation may not have enough angular resolution. Special relativity should be also taken into account before any definite claim is made. As the angular momentum prior to the collapse increases, the dynamics becomes closer to MF3. The jet is commonly generated in the direction of the rotational axis and the aspect ratio gets smaller as the rotation becomes faster. The explosion energy and the ejected mass are gradually decreased to those of MF3 as summarized in Table 2.

Finally, Model MF8 is run to study the case with a very rapid rotation and a weak magnetic field, the opposite extreme of Model MF5. The result is essentially the same as other magneto-rotational models. The dynamics is quite similar to the pure rotation Model

MF2 at first. Then the toroidal field is amplified around the inner core surface and finally the jet is launched from that region. The difference of the initial magnetic field strength is reflect by the time it takes the jet to be produced by the magnetic fields. The explosion energy and the ejected mass are moderate. It seems that the combination of slow rotation and large magnetic field is better for the prompt explosion than the opposite combination. It should be noted that our computation is limited to the prompt explosion time scale and the magnetic fields considered here are all very strong (this is true even for MF8. See Heger et al. (2003)). The amplification of even smaller magnetic fields on a longer time scale may be possible (Akiyama et al. 2003) and important, since the explosion will be delayed in the neutrino heating mechanism if it works at all (Rampp and Janka 2000; Liebendörfer et al. 2001; Thompson et al. 2003).

3.2. angular momentum and magnetic field amplification

The jet we have commonly seen in the previous section is generated in the region where substantial toroidal fields are produced from the initial poloidal fields by differential rotations. This is the region between the shock wave and the boundary of the inner core and the outer core near the rotation axis. In the inner core, matter infall approximately in a homologous way ($v \propto r$), while the outer core collapses like a free fall ($v \propto r^{-1/2}$). As a result, the differential rotation is strongly enhanced not in the inner core but in the outer core. Since matter fall more rapidly near the rotation axis, unhindered by the centrifugal force, the differential rotation is larger in the vivinity of the rotation axis (Akiyama et al. 2003). Fig. 10 shows the degrees of differential rotation for Models MF3 and MF5 at $\sim$ 6ms after the bounce. In both models, the shock wave is located at $r \sim$ 130km. It is clear that the contour levels are dense not only in the inner core but also around the boundary of the inner and outer cores as stated above. This is a feature common to all the models. This is also confirmed by the fact that the angular momentum is most efficiently transported by magnetic fields there. In Fig. 11 we show the cumulative distribution of specific angular momentum, $j(m)$, for Model MF3. In the axisymmetric hydrodynamic collapse, each fluid element preserves its specific angular momentum regardless of its motions, since the axisymmetric pressure wave does not transport angular momentum. As a result, the mass of the fluids with a specific angular momentum smaller than a particular value, $m(< j)$, is a constant of motion. Hence the cumulative distribution function $j(m)$ which is an inverse function of $m(< j)$ is also unchanged in time for the current case (Yamada and Sato 1994). This is not the case, however, for the magnetohydrodynamic collapse, in which the magnetic stress changes the specific angular momentum of each fluid element even in axisymmetry if the fluid rotates differentially. Hence the time variation of the specific angular momentum

distribution can be used as a measure of differential rotations. Note that since the specific angular momentum is a monotonically increasing function of the distance from the rotation axis, the cumulative mass serves, crudely speaking, as a mass coordinate like in the spherical collapse. Incidentally, this monotonically increasing angular momentum distribution is stable against the so-called Rayleigh instability (Tassoul 1978). As evident in the figure, the angular momentum is efficiently transferred from $\sim 0.7 M_\odot$ to $\sim 1.1 M_\odot$ in the mass coordinate defined above. Since, the inner core mass is $\sim 0.74 M_\odot$ for this model (see Table 2), this roughly corresponds to the region outside the boundary of the inner and outer cores. This is a feature common to all the models.

The strong differential rotation induces toroidal fields from poloidal ones. This is seen in Fig. 12, where shown are the contours of the ratio of the toroidal magnetic field pressure to the matter pressure for Models MF3 and MF5 together with the angular velocity contours. The ratio becomes as high as 10% or more and the magnetic stress is a driving force of the jet we have seen. In fact, the jet is sometimes produced slightly off axis at the region where the ratio of the pressures becomes maximum. The amplification of the toroidal fields is enhanced by lateral motions of fluids, which are accompanied by the deformation of the poloidal fields as evident in the bottom panels of Fig. 6. It is easily understood that this stretching of the poloidal fields enhances the amplification of the toroidal fields, since the angular velocity at the start point is considerably different from that at the end point of the lateral motion. This is particularly important for almost vertical poloidal fields as we assumed for the initial state. There seems to be two factors causing this lateral motion, and which is more important depends on the shock strength. The first one is the oblique shock, which tends to deflect matter away from the rotation axis as seen, for example, in the upper panels of Fig. 6. It should be noted that the lateral motion behind the shock wave is especially remarkable for the MS sequence in which the prompt shock is very energetic. In this case, the region with a large ratio of magnetic pressure to matter pressure prevails widely behind the shock. Although this is more so for the combination of strong magnetic field and very rapid rotation, the lateral motion occurs even in the non-rotation case (see Fig. 8).

The lateral stretching of the poloidal fields also occurs much behind the shock wave. This is more evident for the MF sequence, in which the prompt shock is weaker, and most clearly seen for the slow rotation model MF5 (see Fig. 9) and the low magnetic field model MF8 (Fig. 13), in which models it takes longer to launch a jet. This lateral motion is apparently not induced by the shock wave but appears to be associated with an instability similar to the so-called magneto-rotational instability (MRI) (Balbus and Hawley 1991; Akiyama et al. 2003). MRI is an instability which differentially rotating magnetized matter may experience. If a fluid element of a magnetized gas in rotational equilibrium is dislocated from its equilibrium

position in the direction perpendicular to the rotation axis which is assumed to be parallel to the magnetid filed, it will not return to the original position if the angular velocity distribution $\Omega(\varpi)$ satidfies $d\Omega(\varpi)/d\varpi < 0$, where ϖ is the distance from the rotational axis. This is because the magnetic field exerts its force to keep the dislocated fluid element to corrotate with the matter at the original position, and the resultant unbalance of the centrifugal force, pressure and gravity, leads to a further deviation from the original position. This motion of the fluid element is accompanied by the amplification of the magnetic field, since it inevitably causes the stretch of the poloidal field in the perpendicular direction, which in turn generates toroidal fields followed by the wrapping. This situation for the MRI is reminescent of the post-bounce configuration of the supernova core considered here. In fact, there are strong differential rotations induced between the shock wave and the boundary of inner and outer cores as well as the poloidal magnetic fields, and there are, indeed, lateral motions (that is, perpendicular to the rotatinal axis) observed in the same region. In models MF5 and MF8, after the lateral motions set in, the toroidal magnetic fields become substantial and the jet is produced there. Note, however, that in our simulations, matter are not in equilibrium and it is very difficult to distinguish the non-radial accretion flow induced by the rotation and the oblique shock wave from the motion induced by the instability, particularly in the early growth phase of the lateral motion. Furthermore, the relatively low angular resolution of our simulations makes it impossible for us to study the linear growth phase to see clearly if the motion is really associated with the MRI. Nevertheless, it will be still useful to look into the growth time scales and the saturation field strengths which the theory of the MRI predicts for the current models. As a typical growth time, we take the following relation from the linear analysis (Akiyama et al. 2003)

$$\tau \ = \ 4\pi \left| \frac{d\Omega}{d \ln \varpi} \right|^{-1} \quad . \tag{14}$$

The inverse of this time scale, or the growth rate, is shown in the lower left panel of Fig. 14 for Model MF8. The time scale is shorter in the region where the lateral motion is later induced. This is the boundary of the inner and outer cores, as repeatedly mentioned. In the region very close to the rotation axis, the time scale becomes larger. This is because the gradient of the angular velocity distribution is oriented approximatedly in the radial direction for this model. It is found that the expected growth time scale is approximately of the same order as the evolution time scale after the bounce, a few tens miliseconds. Note, however, again that the linear growth rate is just a rough measure of the non-linear motion we are actually observing in the simulations. The strength of the saturation magnetic fields is difficult to estimate, since it cannot be obtained from the linear analysis. We take here also an order-estimate approach and adopt the prescription (Akiyama et al. 2003)

$$B_{sat}^2 \ = \ 4\pi \rho v_\phi^2 \quad . \tag{15}$$

In the lower right panel of Fig. 14, we show the squared ratio, $(B_\phi/B_{sat})^2$, of the computed toroidal magnetic field to the saturation field given by Eq. (15). It is seen that the field strength obtained in the simulations are comparable to or greater than the expected saturation values in the region where the lateral motion is induced and, as a result, the toroidal magnetic fields are amplified. Note that even Model MF8 with the weakest magnetic field of our models is assumed to have large magnetic fields, $\sim 10^{12}$G, from the beginning of collapse. Hence it is of great importance to see if the mechanism of the field amplification and the subsequent jet formation discussed here is taken over to the case with much smaller magnetic fields prior to the collapse (Akiyama et al. 2003). It should be also added that the saturation of MRI, if it really grows, is itself a very important issue and should be studied further along with its linear growth in the current context, and will be a future work.

3.3. gravitational wave form

Here we look into the gravitational wave forms, which are remarkable mainly around the core bounce. As shown in Eq. (13), there are three contributions to the wave. The first is the hydrodynamic part, the second is $\boldsymbol{j}\times\boldsymbol{B}$ part and the third part comes from the time derivatives of the energy density of electro-magnetic field. Since the energy density is dominated by matter, the last part is much smaller than the others. In Fig. 15, we show the results of Models MS3 and MF3 together with the corresponding pure rotation models MS2 and MF2. The burst feature is apparent in the figure. This corresponds to the core bounce at which time the most dynamic change of the mass quadrupole of the system occurs. It is also clear that the difference is minor between the pure rotation models and the magneto-rotational models. This is not unexpected. As shown in Table 2, the mass density is almost identical for the pure rotation models and the magneto-rotational models at the core bounce. This is mainly due to the fact that the initially uniform magnetic fields do not have a large fraction of energy in the inner core region. That is also the reason why the ratio of the energy of magnetic field to the gravitational energy becomes smaller around the core bounce than at the beginning. Hence if we consider different initial configurations of magnetic field, in particular, the ones with centrally concentrated fields, more substantial difference will show up. For the models considered in this paper, however, it is difficult to detect magnetic fields of supernova cores via the gravitational radiations.

The feature in the gravitational waves for Models MF6 and MF7 presented in Fig. 16, is essentially that for the rotational collapse. As the rotation gets slower, the duration of the burst becomes shorter, since the dynamical time scale is smaller due to larger density. Note that the width of the burst is mainly determined by the average density of the inner

core at the core bounce (Yamada and Sato 1995). The amplitude is a little bit greater for MF6. The peak amplitudes are $\gtrsim 10^{-21}$ if an observer is located on the equatorial plane 10kpc away from the source. The frequencies are typically a few hundreds Hz.

Non-rotation model MF4 is qualitatively different from others. In this model, the magnetic field is the sole cause for the anisotropic dynamics. As depicted in Fig. 17, the gravitational waves are emitted substantially around the core bounce also in this case. The negative amplitude for the first peak implies that the inner core is oblate at the bounce as in rotational cases. An interesting feature is that the second peak with a positive amplitude is as remarkable as the first one. This is in contrast with other models, for which the second peak is substantially minor. This reflects the difference of the oscillations of the inner core after bounce. The rapidly rotating core tends to oscillate with larger amplitudes compared with the spherical case in which smaller oscillations are quickly damped. In this respect the Model MF4 is closer to the spherical bounce. The wave form for Model MF5 is already quite different from that of MF4 as evident from Fig. 17. This means that the models considered in this paper are all rapid rotators. In fact, although the initial $|T/W|$ is 0.1% for Model MF5, the amplitude of the burst is comparable to other more rapidly rotating models. It is noted that the vertical scales are different by an order of magnitude for MF4 and other models. Hence, although the wave form is qualitatively different, it is unlikely that the gravitational radiation from a magnetized non-rotating supernova will be observed in the near future unless the configuration of magnetic field is quite different from the one considered here.

4. Discussion and Conclusion

We have done a systematic 2D numerical study of the magneto-rotational collapse and subsequent shock propagation in the supernova core on the prompt explosion time scale. With the assumption that the initial rotation is uniform and the magnetic field is constant in space and parallel to the rotation axis, the strength of rotation and magnetic field is varied arbitrarily and 12 models have been computed to investigate the systematics of the dynamics. The complicated matter EOS and the neutrino transport are mimiced by the simplified parametric EOS we adopted in this paper, and the dependence of the dynamics on one of these parameters, Y_l, has been also studied. It is emphasized that there have been only a few simulation models computed so far (Symbalisty 1984). Hence it is important to increase the number of models and broaden the investigated parameter region to obtain the generic trend of the dynamics. Given this scarcity of magnetic supernova models compared with spherical symmetric models or even with non-magnetic rotational models, we think

that we had better start our investigation with the dynamics on the prompt explosion time scale.

For the trapped lepton fractions, we have adopted larger (0.38) and smaller (0.35) values. In the former case, the prompt shock is strong enough to propagate through the entire core and lead to a prompt explosion even in the non-rotation model, while in the latter the shock wave is weaker and no explosion occurs both for non-rotation and rotation models. From recent realistic 1D simulations of collapse-driven supernovae (Rampp and Janka 2000; Liebendörfer et al. 2001; Thompson et al. 2003), we think the latter case is more realistic than the former. Nonetheless, we have studied both cases for completeness and comparison. We have found that the rotational models, when combined with magnetic fields, give jet-like prompt explosions for both of the trapped lepton fractions. Although this result seems similar to those found in LeBlanc and Wilson (1970) or Symbalisty (1984), the driving force of the jet-like explosion in our models originates from the the magnetic fields in the outer core, the region between the shock wave and the inner core unlike LeBlanc and Wilson (1970) or Meier et al. (1976), in which the authors discussed mainly the magnetic fields in the inner core. Furthermore, the amplification of magnetic fields in this region occurs differently according to the shock strength. For stronger shocks (due to the larger Y_l), the magnetic fields are amplified by the strong differential rotation and further enhanced by lateral motions of fluid which are induced chiefly by the oblique shock. For weaker shocks with the smaller Y_l, on the other hand, the significant amplification of magnetic fields occurs in a narrower region much behind the shock wave, where it seems that the lateral motions are induced not by the oblique shock wave but by the MRI-like instability.

It should be noted that we assumed in this paper that the stellar core has large magnetic fields ($\sim 10^{12}$G) prior to the collapse (see Table 1). It is admittedly difficult to justify this assumption either by observations or by theoretical studies at present. In particular, the simultaneous realization of rapid rotation and strong magnetic field seems difficult, since the magnetic torque will then slow down the rotation substantially. This is suggested by recent stellar evolution models (Heger et al. 2003). Hence we should regard our models as an extreme limit, applicable probably for the magnetars. The initial configuration of the magnetic field, assumed uniform and parallel to the rotation axis in this paper, has no firm grounds, either. Probably, the magnetic field energy will be more concentrated in the central part of the core prior to the collapse and not only poloidal fields but also comparable toroidal fields will be prevalent in the core (Spruit 2002). Note that the uniform magnetic field we take as an initial condition in this study has a large fraction of energy in the outer portion of the core and, as a result, it tends to affect the matter dynamics more strongly as the shock wave propagates outwards. Provided the paucity of theory or observation, we think that the best we can do at the moment is a systematic parametric research. In this respect, this

paper covers a small (and rather extreme) part of the parameter space and is just a starter and a more thorough study is currently underway (Sawai and Yamada 2004), in which the initial angular momentum distributions and configurations of magnetic fields are varied more widely. The input micro physics should be also sophisticated, since the approximation of the post bounce dynamics by the thermal stiffness is certainly a very crude approximation.

In the current study, as mentioned above, we have in mind magnetars, a neutron star which has much larger magnetic fields than ordinary radio pulsars and might form a minor sub-group of neutron stars (Zhang and Harding 2000; Guseinov et al. 2003). It is beyond the scope of this paper to address the mechanism of the ordinary collapse-driven supernova which will lead to the formation of the ordinary pulsars. However, there is an attempt to consider the magneto-rotational collapse as more general a mechanism for the collapse-driven supernovae (Wheeler et al. 2002; Akiyama et al. 2003). In their models, MRI is supposed to grow rapidly and amplify initially small magnetic fields in the core, followed by a successful, probably jet-like, explosion. In this respect, Model MF8 with the smallest initial magnetic field of our models might be interesting. Although the initial magnetic field of this model is still very large compared with the value supposed in (Akiyama et al. 2003), the post bounce dynamics is at first little affected by the magnetic fields and very similar to the rotation-only model. Then the lateral motions are induced possibly by the MRI-like instability much behind the shock wave, accompanied by the lateral stretch of the poloidal magnetic fields and amplification of toroidal fields, which in turn produce the jet in the direction of the rotation axis. The dynamics becomes very similar to other models with larger magnetic fields later on. If this behavior is taken over to much smaller magnetic fields ($\sim 10^9$G) as predicted by the recent evolution model (Heger et al. 2003), it might be a promising alternative to the current neutrino paradigm (Wheeler et al. 2002; Akiyama et al. 2003). In fact, since the neutrino heating requires some time ($\sim$a few hundreds miliseconds) before the stalled shock is revived, the amplification of the magnetic fields by MRI has a lot of available time, if it really grows. The delay of explosion due to the amplifacation of magnetic fields might be advantageous for making a massive enough neutron star, since the prompt explosion tends to leave behind a smaller neutron star unless a substantial fallback ensues. Putting aside if MRI really grows in the supernova core, we do not know either at present if MRI alone can lead to a successful explosion or the combination with the anisotropic neutrino irradiation (Shimizu et al. 2001; Kotake et al. 2003) is needed. Even if MRI successfully yields an explosion, we will have to see if the canonical value of the surface magnetic fields can be obtained for most of neutron stars. These issues definitely need further studies, possibly by 3D numerical simulations, since the instability will occur with no particular symmetry.

In the connection to GRB, it is interesting that the combination of a slow rotation and a strong magnetic field (Model MF5) produces a very collimated but still powerful jet-like

explosion. The matter velocity becomes almost half the light velocity. While the aspect ration of the shock wave is ~ 2 in other models, it is about 5 in MF5. The small rotation allows to form a compact core and, as a result, the amplification of the magnetic field is confined to a smaller region, leading to the very collimated jet. It is noted again that the recent stellar evolution models suggest smaller angular momenta than previously thought for pre-collapse cores if magnetic fields are taken into account (Heger et al. 2003) (note, however, that the initial magnetic field of MF5 is much larger than predicted). Since our code is Newtonian and the angular resolution is rather poor, the relativistic narrow jet found in MF5 should be regarded as a preliminary result and needs further study with a general relativistic MHD code (see, for example, (Mizuno et al. 2004)). The general relativity will give a correction of $\lesssim 10\%$ to the Newtonian dynamics studied in this paper.

It is almost mandatory for a multi-dimensional study of supernova to address the gravitational radiation. So far no author has discussed the gravitational waves emitted from the MHD collapse and bounce of the supernova core except for our companion paper (Kotake et al. 2004), which mainly discusses the toroidal fields and is complementary to this paper. We have found in this paper that the gravitational radiations from a magnetized non-rotating star are unique in wave form (see the left panel of Fig. 17). The common negative trough is followed by a positive peak with a similar absolute amplitude. This reflects the difference of the post bounce oscillations of the inner core. In this respect, the magnetized non-rotating core is more like a spherical core. Although the wave form is qualitatively different from the rotational cases, it is unlikely to be observed even if the source is located at a distance of $\sim$10kpc from us, since the amplitude is lower by an order of magnitude than for the rotational models. The rotation energy as small as $|T/W| \sim 0.1\%$ already changes the wave form to that typical for the rotational collapse. This is understandable from the fact that the gravitational wave is emitted as a burst mainly from the core bounce, at which time the magnetic field plays essentially no role in dynamics. This may be changed, however, if different initial configurations of magnetic fields are considered. Particularly, more centrally concentrated magnetic fields might make some imprint in the gravitational radiations. This is also currently being investigated and will be presented elsewhere (Sawai and Yamada 2004).

Bearing in mind the origin of the very strong magnetic fields inferred for magnetar, we have studied in this paper magneto-rotational core collapses in the extreme parameter regime. Although this will not be a mechanism of the ordinary collapse-driven supernova, we think it is important to extend the parameter region further to assess how generic is the feature of the dynamics we have found in this paper, which, we hope, will lead to some insight of the mechanisms of the ordinary supernova as well as GRB.

This work was partially supported by the Grants-in-Aid for scientific Research (14740166, 14079202) of the ministry of Education, Science, Sports and Culture of Japan. Some of the numerical simulations were done on the supercomputer VPP700E/128 at RIKEN and VPP500/80 at KEK (KEK Supercomputer Projects No.02-87 and No.03-92).

REFERENCES

Akiyama, S., Wheeler, J. C., Meier, D. L. and Lichtenstadt, I. 2003, ApJ, 584, 954

Ardeljan, N., V., Bisnovatyi-Kogan, G. S. and Popov, Ju. P. 1979, AZh, 56, 1244

Ardeljan, N. V., Bisnovatyi-Kogan, G. S. and Moiseenko, S. G. 2000, A&A, 355, 1181

Balbus, S. A. and Hawley, J. F. 1991, ApJ, 376, 214

Bisnovatyi-Kogan, G. S., Popov, Iu. P. and Samokhin, A. 1976, Ap&SS, 41, 287

Blanchet, L., Damour, T. and Schäfer, G. 1990, MNRAS, 242, 289

Chevalier, R. A. and Soker, N. 1989, ApJ, 341, 867

Finn, L. S. and Evans, C. R. 1990, ApJ, 351, 588

Guseinov, O. H., Yazgan, E., Ankay, A. and Tagieva, S. 2003, Int. J. Mod. Phys., D12, 1

Heger, A., Fryer, C. L., Woosley, S. E., Langer, N. and Hartmann, D. H. 2003, ApJ, 591, 288

Heger, A., Woosley, S. E., Langer, N. and Spruit, H. C. 2003, in Proc. IAU 215 "Stellar Rotation", astro-ph/0301374

Ishikawa, S., Yamada, S., Kiguchi, M. and Sato, K. 1992, A&A, 258, 415

Janka, H.-Th. and Mönchmeyer, R. 1989, A&A, 226, 69

Khokhlov, A. M., Höflich, P. A., Oran, E. S., Wheeler, J. C., Wang, L. and Chtchelkanova, A. Yu. 1999, ApJ, 524, L107

Kotake, K., Yamada, S. and Sato, K. 2003, ApJ, 595, 304

Kotake, K., Yamada, S., Sato, K., Sumiyoshi, K., Ono, H. and Suzuki, H. 2004, Phys. Rev. Din press

LeBlanc, J. M. and Wilson, J. R. 1970, ApJ, 161, 541

Leonard, D. C., Filippenko, A. V. and Matheson, T. 2000, in Cosmic Explosions! Proc. 10th Maryland Conf. Astrophys., ed. S. S. Holt and W. W. Zhang (New York : AIP)

Liebendörfer, M., Mezzacappa, A., Thielemann, F. -K., Messer, O. E., Hix, W. R. and Bruenn, S. W. 2001, Phys. Rev. D63, 103004

MacFadyen, A. and Woosley, S. E. 1999, ApJ, 524, 262

Meier, D. L., Epstein, R. I., Arnett, W. D. and Schramm D. N. 1976, ApJ, 204, 869

Mizuno, Y., Yamada, S., Koide, S. and Shibata, K. 2004, ApJin press

Mönchmeyer, R. and Müller, E. 1989, in Timing Neutron Stars, eds. H. Ögelman and E. van den Heuvel, (Dordrecht : Kluwer Acad. Publishers)

Mönchmeyer, R., Schäfer, G., Müller, E. and Kates, A. E. 1991, A&A, 246, 417

Müller, E. and Hillebrandt, W. 1979, A&A, 80, 147

Ohnishi, T. 1983, Tech. Rep. Inst. At. En. Kyoto Univ. No.198

Rampp, M. and Janka, H. -Th. 2000, ApJ, 539, L33

Sawai, H. and Yamada, S. 2004, in preparation

Shapiro, S. L. and Teukolsky, S. A. 1983, Balck Holes, White Dwarfs, and Neutron Stars, (New York : A Wiley-Interscience Publications)

Shimizu, T., Yamada, S. and Sato, K. 1994, ApJ, 432, L119

Shimizu, T. M., Ebisuzaki, T., Sato, K. and Yamada, S. 2001, ApJ, 552, 756

Spruit, H. C. 2002, A&A, 381, 923

Stanek, K. Z. et al. 2003, ApJ, 591, L17

Stone, J. M. and Norman, M. L. 1992, ApJS, 80, 791

Symbalisty, E. M. D. 1984, ApJ, 285, 729

Takahara, M. and Sato, K. 1984, Prog. Theor. Phys., 71, 524

Tassoul, J.-L. 1978, Theory of Rotating Stars (Princeton : Princeton University Press)

Thompson, T. A., Burrows, A. and Pinto, P. A. 2003, ApJ, 592, 434

Thompson, C. and Duncan, R. C. 1996, ApJ, 473, 322

Wang, L., Wheeler, J. C., Li, Z. and Clocchiatti, A. 2000, ApJ, 467, 435

Wang, L., Wheeler, J. C., Höflich, P., Khokhlov, A., Baade. D. et al. 2002, ApJ, 579, 671

Wheeler, J. C., Yi, I., Höflich, P. and Wang, L. 2000, ApJ, 537, 810

Wheeler, J. C., Meier, D. L. and Wilson, J. R. 2002, ApJ, 568, 807

Woosley, S. E. 1993, ApJ, 405, 273

Woosley, S. E. 1995, private communication

Woosley, S. E. and Heger, A. 2003, in Proc. IAU 215 "Stellar Rotation", astro-ph/0301373

Yamada, S. and Sato, K. 1994, ApJ, 434, 268

Yamada, S. and Sato, K. 1995, ApJ, 450, 245

Zhang, B. and Harding, A. K. 2000, ApJ, 535, L51

Zwerger, T. and Müller, E. 1997, A&A, 320, 209

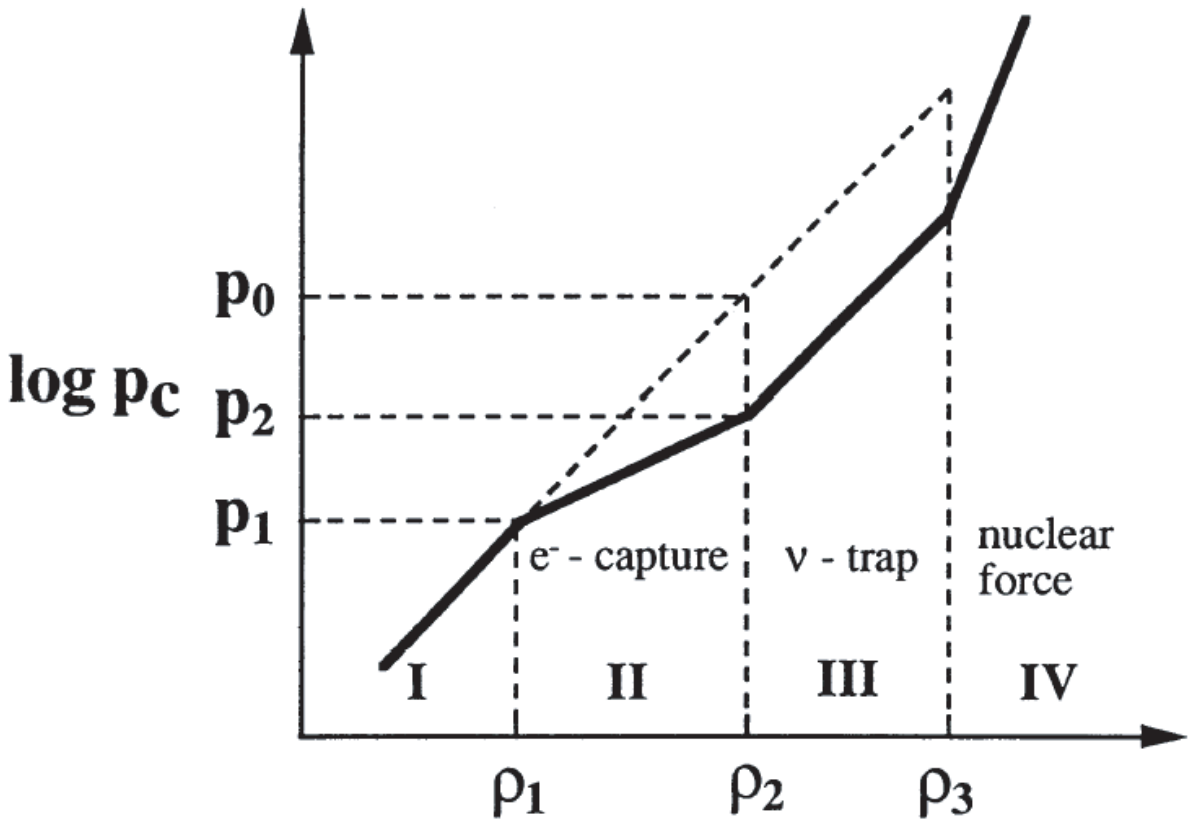

Fig. 1.— The cold part of the parametric EOS. The details are given in the main body.

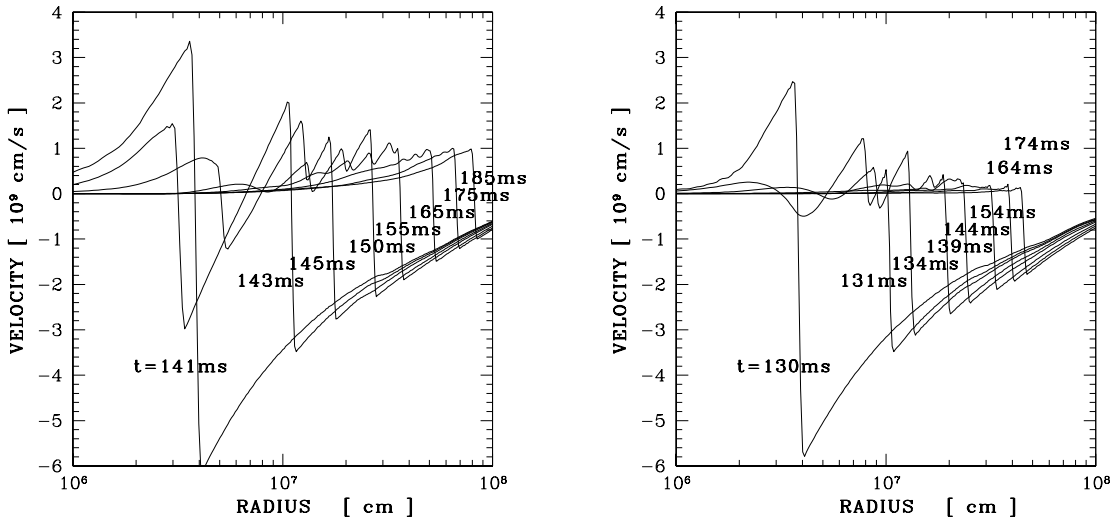

Fig. 2.— The propagations of the prompt shock waves for the spherically symmetric models. Model MS1 has a larger $Y_l = 0.38$ and shows a successful prompt explosion, while Model MF1 with a smaller $Y_l = 0.35$ fails to explode.

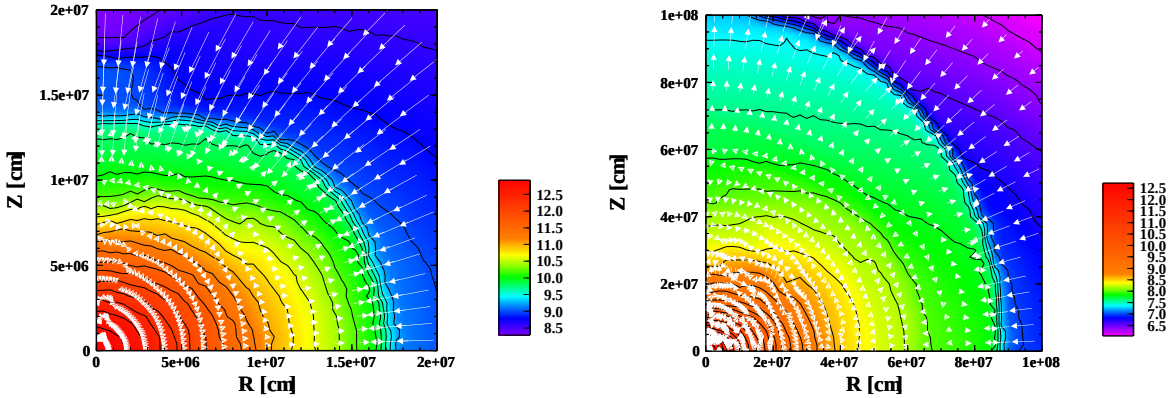

Fig. 3.— The velocity field on top of the density contour for pure rotation case, MS2, at $t = 197$ms (left panel) and $t = 265$ms (right panel).

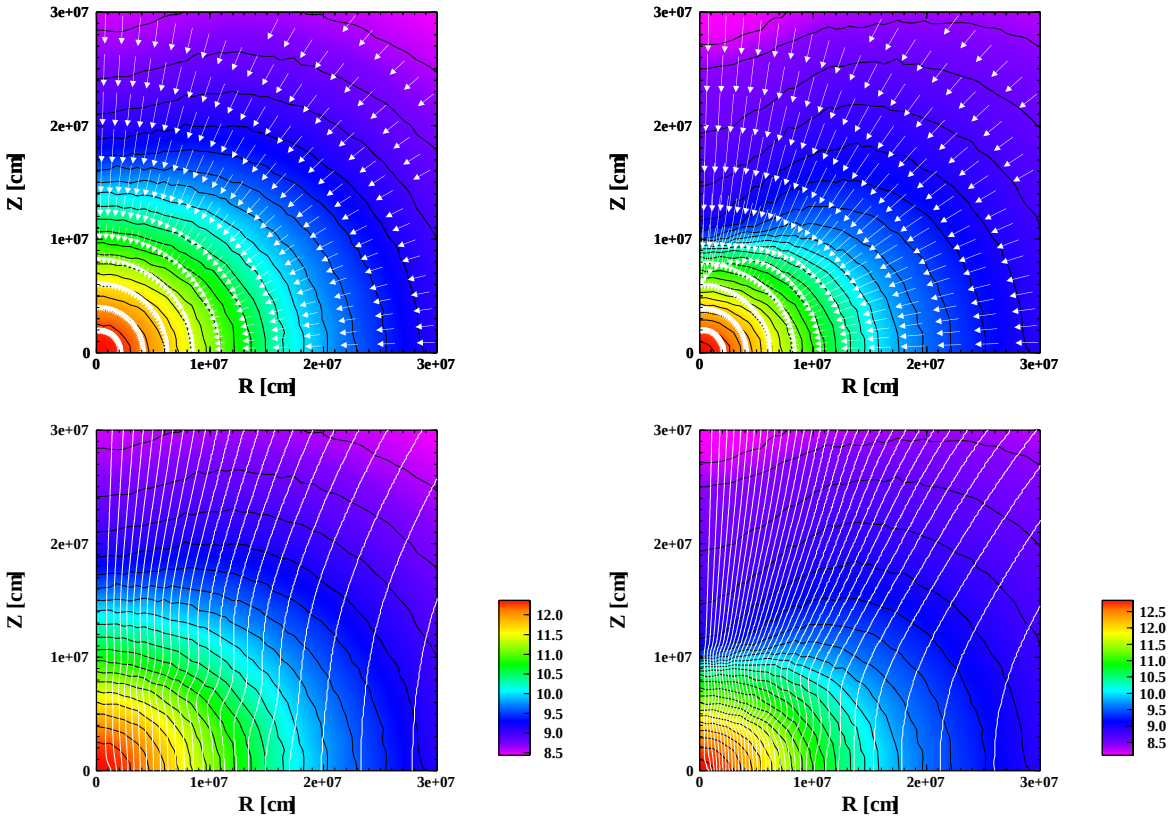

Fig. 4.— The velocity fields (top panels) and the poloidal magnetic fields (bottom panels) on top of the density contours for MS4. The left panels are shown for $t = 183$ms and the right ones for $t = 188$ms.

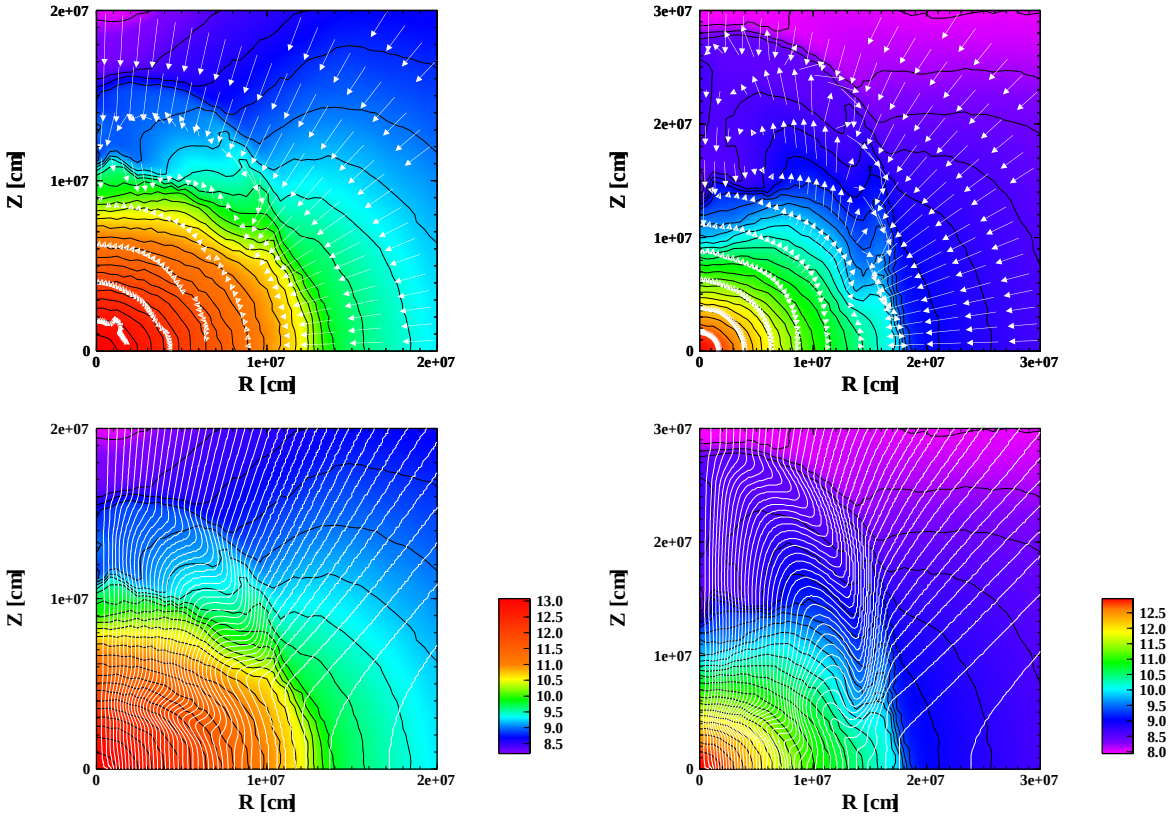

Fig. 5.— The same as Fig. 4. The left panels are shown for $t = 193$ms and the right ones for $t = 198$ms.

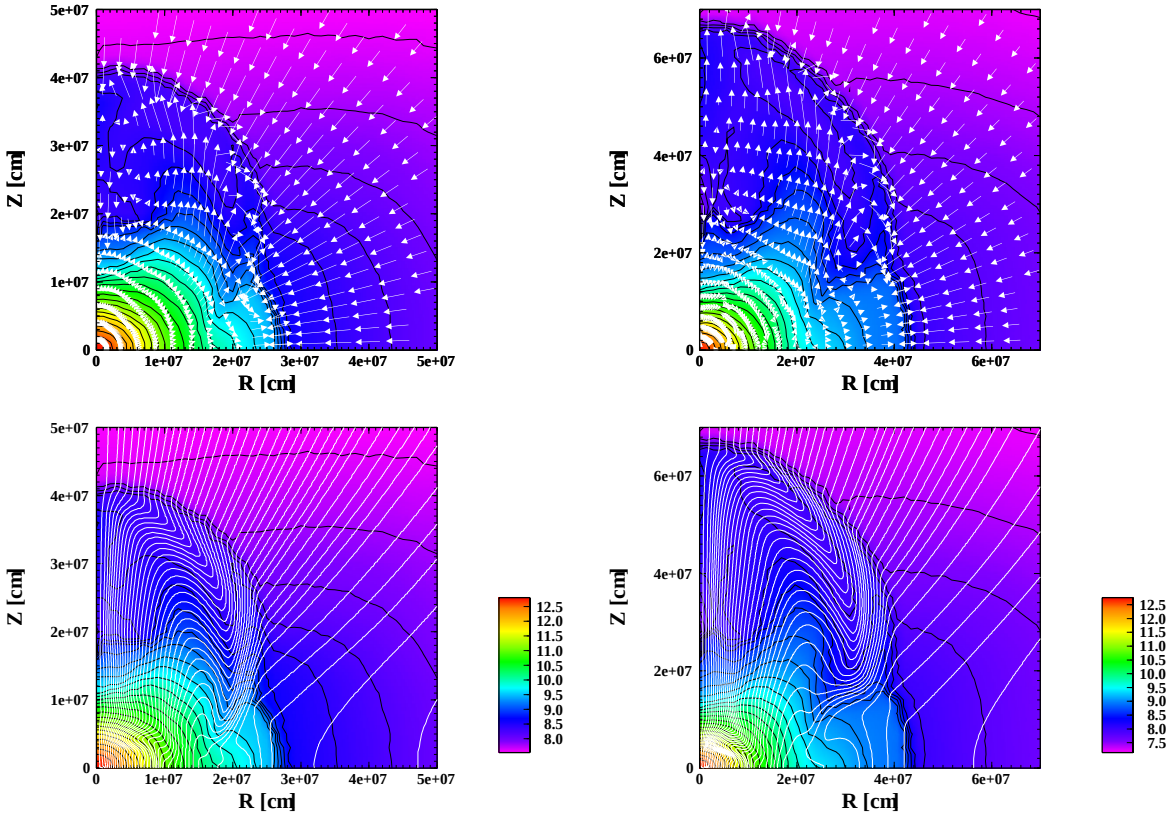

Fig. 6.— The same as Fig. 4. The left panels are shown for $t = 203$ms and the right ones for $t = 213$ms.

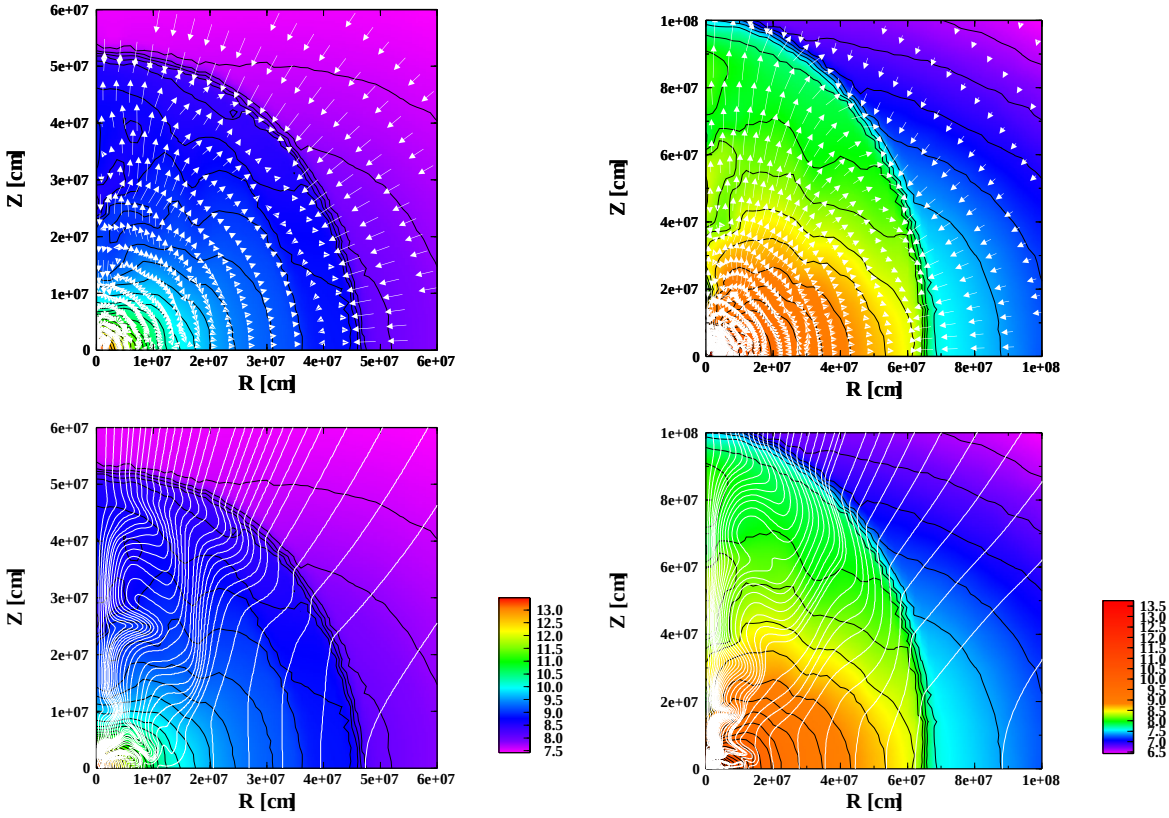

Fig. 7.— The same as Fig. 6 but for model MF3. The left panels are shown for $t = 200$ms and the right ones for $t = 224$ms.

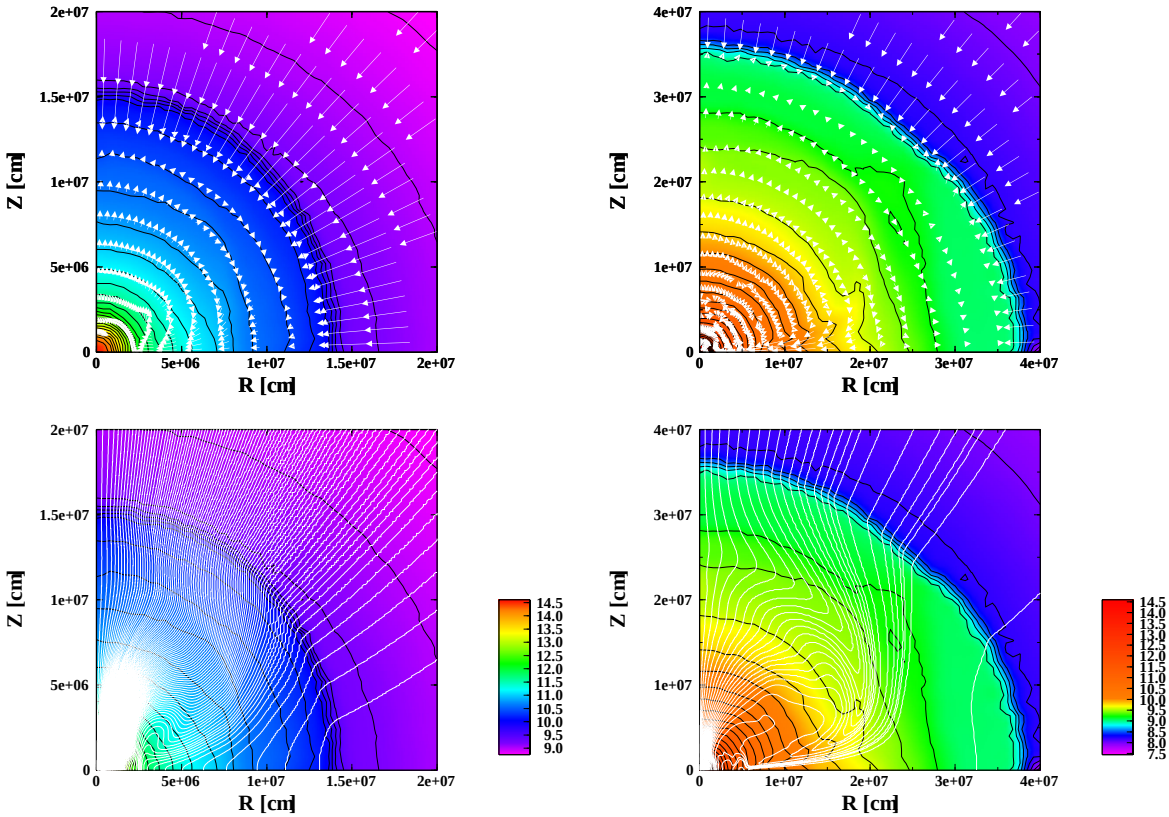

Fig. 8.— The same as Fig. 6 but for model MF4. The left panels are shown for $t = 145$ms and the right ones for $t = 165$ms.

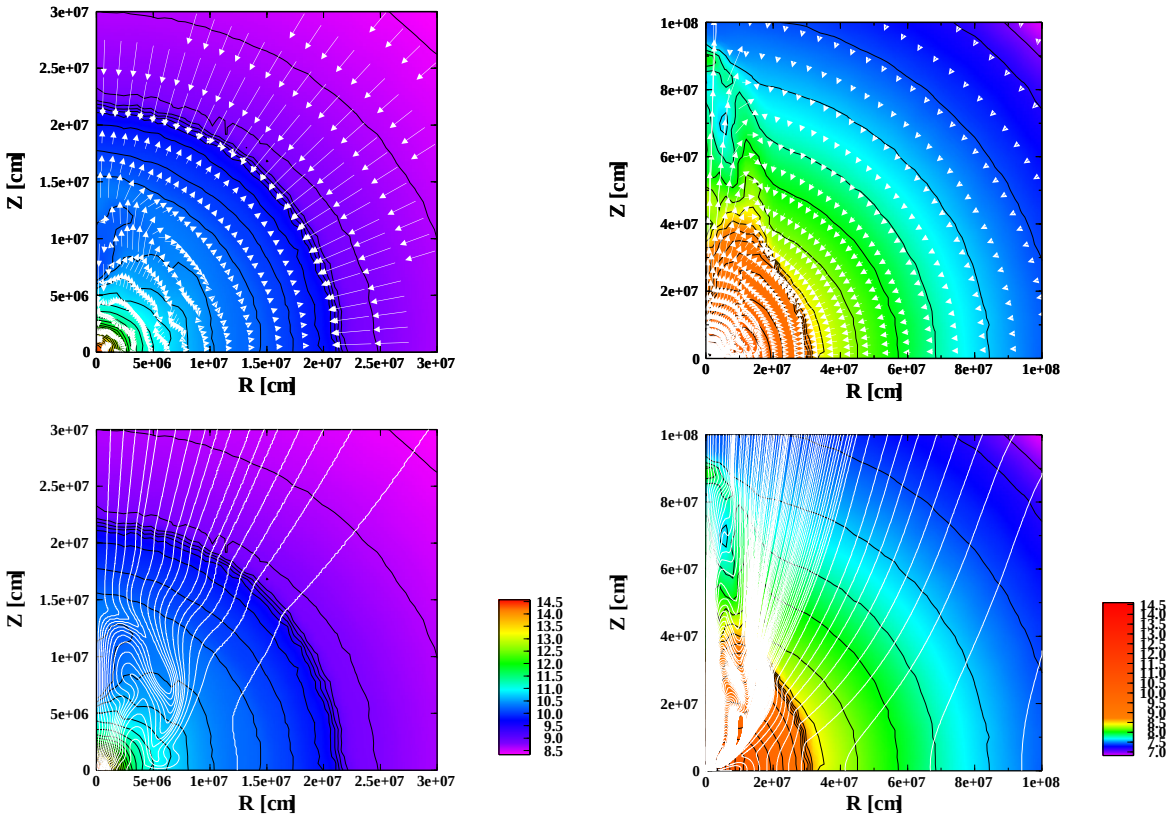

Fig. 9.— The same as Fig. 6 but for model MF5. The left panels are shown for $t = 150$ms and the right ones for $t = 159$ms.

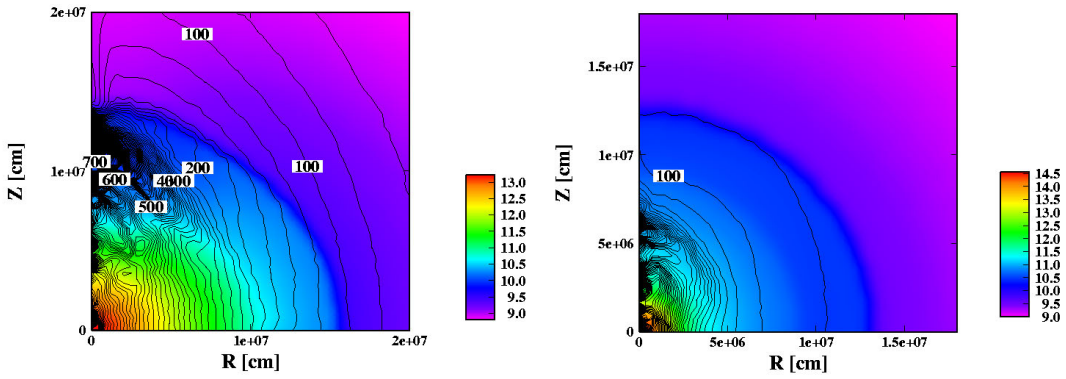

Fig. 10.— The angular velocity contours on top of the density color maps. The left panel shows the distribution for Model MF3 at 174ms ($\sim$ 6ms after bounce) while the right panel gives the corresponding result for Model MF5 at 142ms (($\sim$ 6ms after bounce).

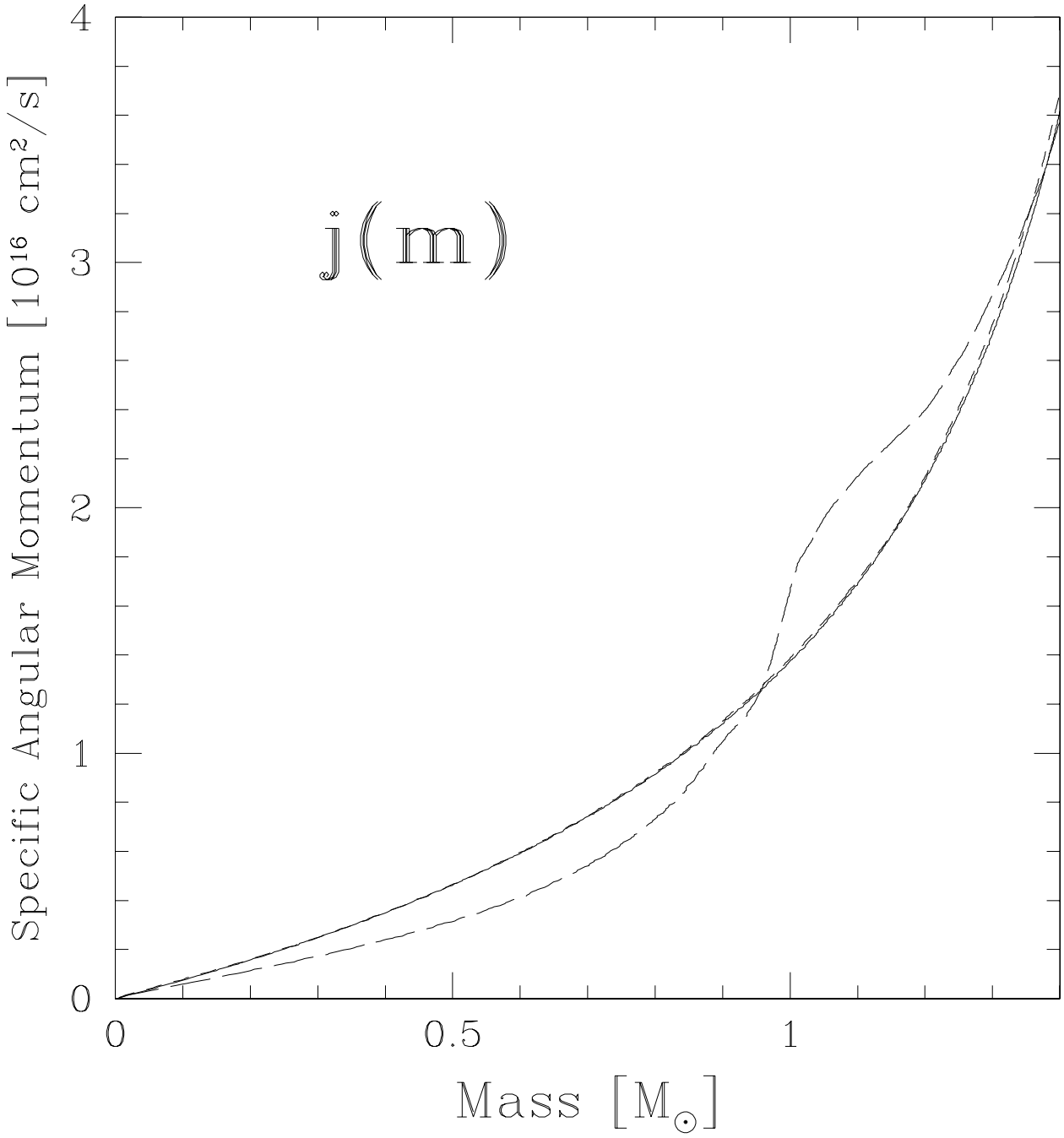

Fig. 11.— The specific angular momentum distribution vs the cumulative mass for Model MF3. The solid line corresponds to the initial distribution, the short dashed line represents the distribution around bounce (t = 174ms) and the long dashed line shows the final distribution (t = 224ms).

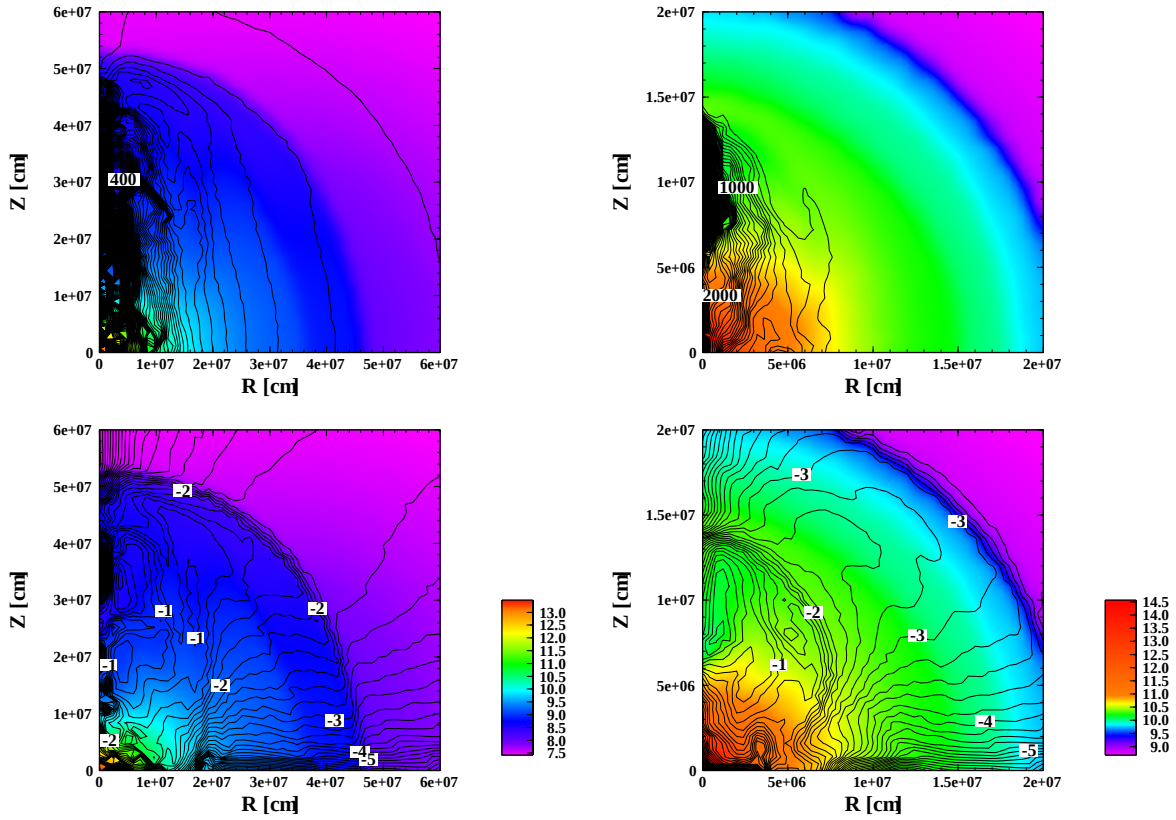

Fig. 12.— The contours of the angular velocity (upper panels) and the ratio of the pressure of toroidal magnetic fields to the matter pressure. The left panels are for Model MF3 (t = 200ms) and the right panels are for Model MF5 (t = 150ms). The lines are drawn for every 10Hz for Model MF3 and for every 100Hz for Model MF5. The logarithm is taken for the pressure ratio. The density is shown in color.

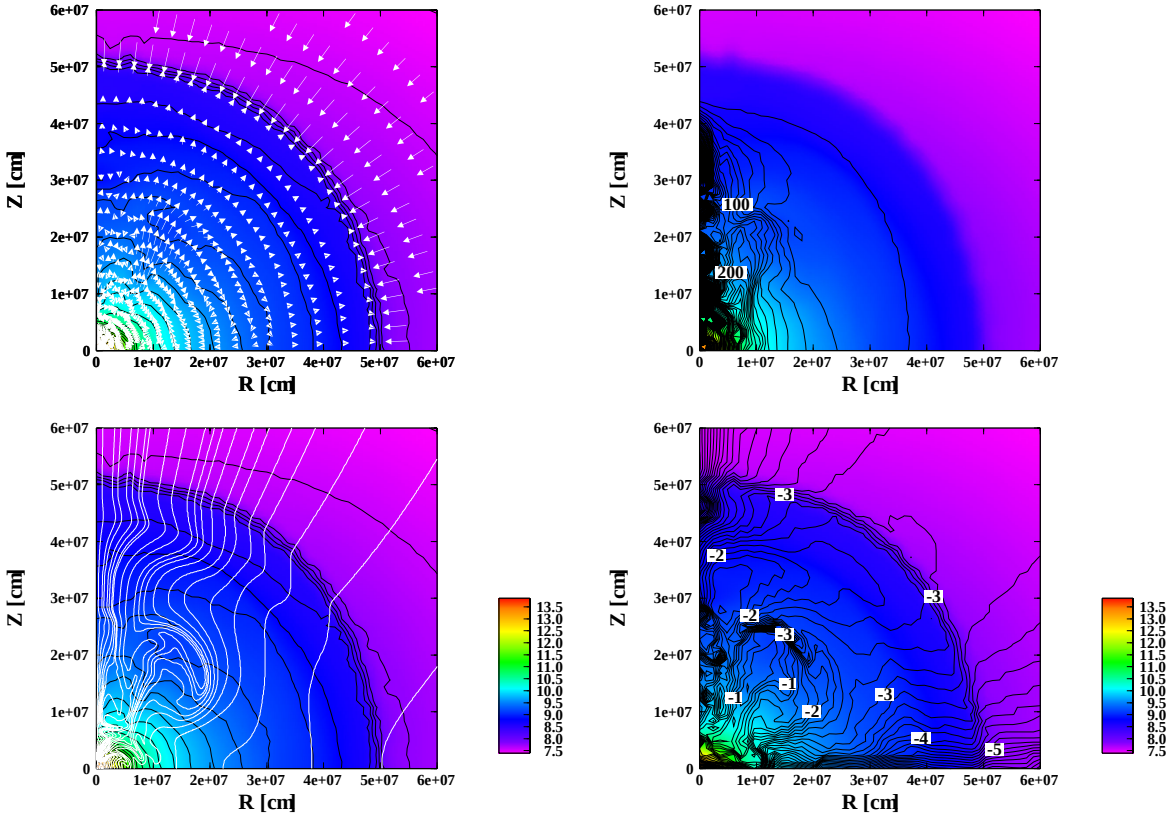

Fig. 13.— The velocity field (upper left panel) and the poloidal magnetic field lines (lower left panel) and the contours of the angular velocity (upper right panel) and the ratio of the pressure of toroidal magnetic fields to the matter pressure (lower right panel) for Model MF8. The time is t = 200ms. The density is shown in color.

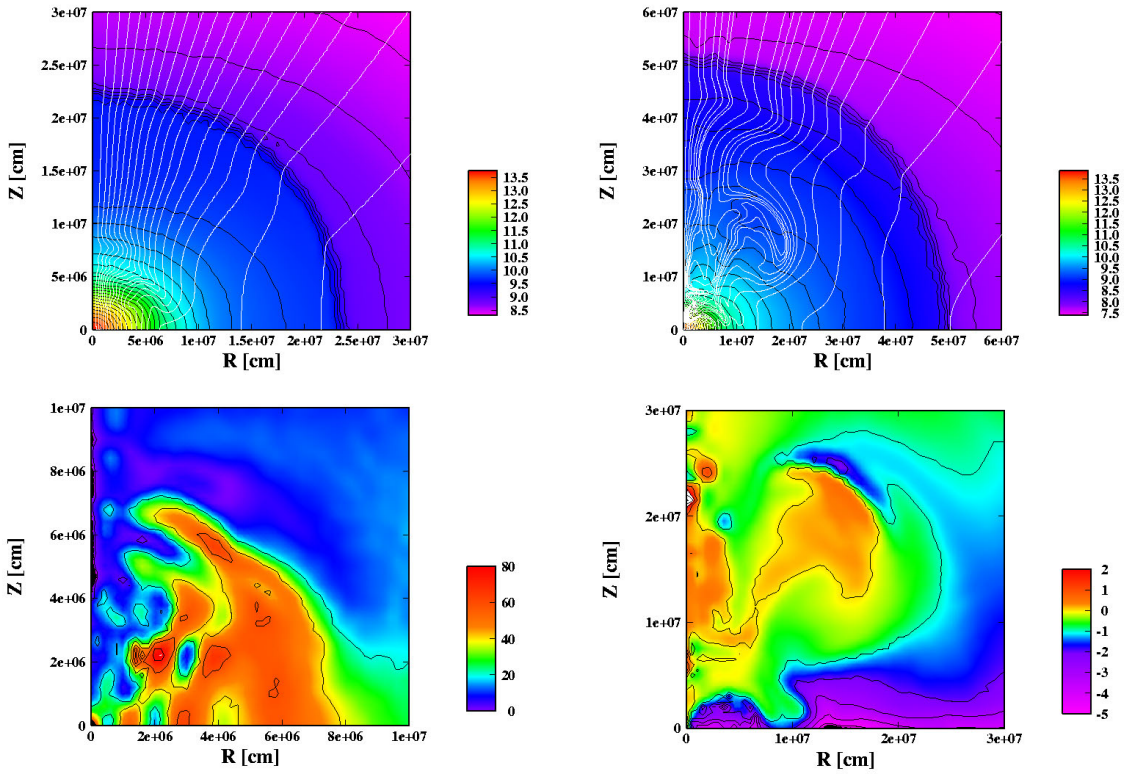

Fig. 14.— The linear growth rate of MRI and the ratio of the toroidal field to the saturation field. The upper left panel shows the poloidal magnetic field on top of the density color map for Model MF8 at 165ms (11ms after bounce). The lower left panel shows the color contour of the growth rate, or the inverse of Eq. (14) at the same time as for the upper left panel. The upper right panel displays the poloidal magnetic field on top of the density color map for the same model at 200ms. The lower right panel presents the color contour map of the squared ratio of the toroidal magnetic field to the saturation field given by, Eq. (15) in the logarithmic scale.

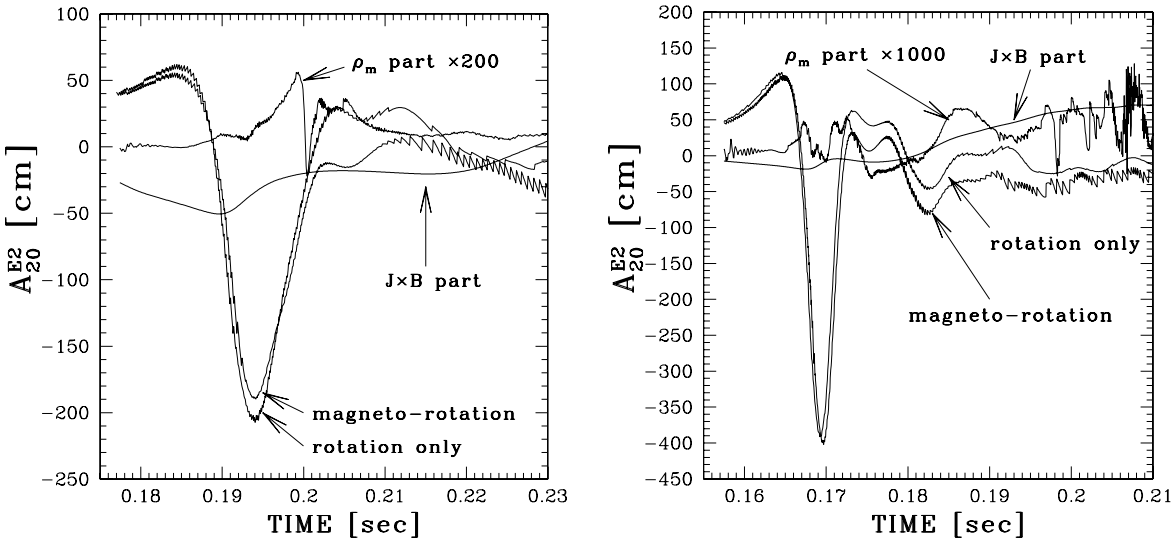

Fig. 15.— The gravitational wave forms for Models MS3 and MF3 together with corresponding rotation-only models MS2 and MF2. The contribution from the magnetic energy density is denoted as ρ_m part and $A^{E2}_{20} = d^2 M^{E2}_{20}/dt^2$.

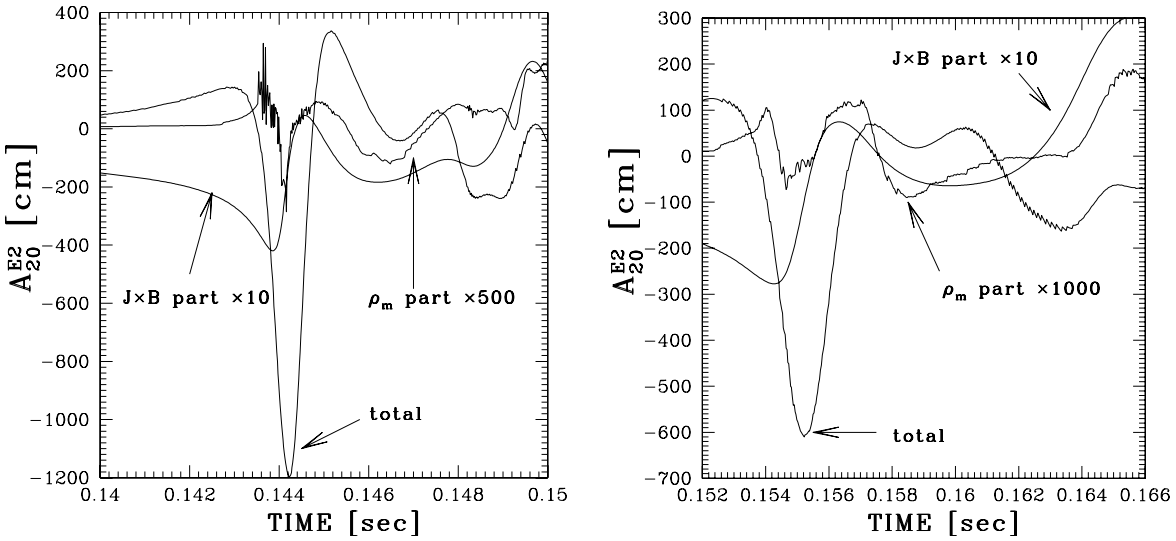

Fig. 16.— The gravitational wave forms for Models MF6 and MF7.

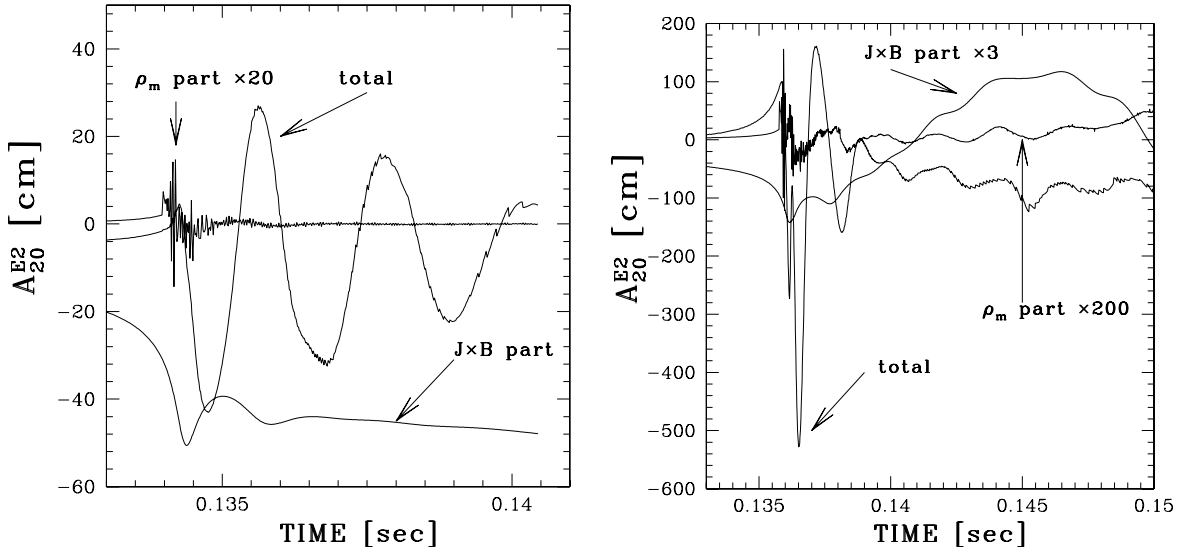

Fig. 17.— The gravitational wave forms for non-rotational MF4 (left panel) and MF5 (right panel). Note the difference of the vertical scale.

Table 1. Model Parameters.

Model	$\|T/W\|$ [%]	Ω_i [rad/s]	$\|E_m/W\|$ [%]	B_i [G]	Y_l
MS1	0	0	0	0	0.38
MS2	1.5	6.8	0	0	0.38
MS3	1.5	6.8	0.5	4.1×10^{12}	0.38
MS4	1.5	6.8	1.0	5.8×10^{12}	0.38
MF1	0	0	0	0	0.35
MF2	1.5	6.8	0	0	0.35
MF3	1.5	6.8	0.5	4.1×10^{12}	0.35
MF4	0	0	0.5	4.1×10^{12}	0.35
MF5	0.1	1.7	0.5	4.1×10^{12}	0.35
MF6	0.5	3.9	0.5	4.1×10^{12}	0.35
MF7	1.0	5.5	0.5	4.1×10^{12}	0.35
MF8	1.0	5.5	0.1	1.8×10^{12}	0.35

Note. — $|T/W|$: the ratio of the rotational energy to the gravitational energy. Ω_i : the initial angular velocity. $|E_m/W|$: the ratio of the magnetic energy to the gravitational energy. B_i : the initial uniform magnetic field. Y_l : the lepton fraction.

Table 2. Key Parameters for All Models.

Model	M_{IC}	ρ_c	$\lvert T/W\rvert_b$	$\Omega_{b,max}$	$\lvert E_m/W\rvert_b$	$B_{b,max}$	$\rho_{c,fin}$	$\lvert T/W\rvert_{fin}$	$\Omega_{fin,max}$	$\Omega_{fin,av}$	$\lvert E_m/W\rvert_{fin}$	$B_{fin,max}$	$B_{fin,av}$	E_{exp}	M_{ej}
MS1	0.84	4.6	0	0	0	0	3.7×10^{14}	0	0	0	0	0	0	2.2	0.42
MS2	0.90	0.11	8.5	2.5×10^{3}	0	0	4.4×10^{12}	7.3	3.7×10^{3}	1.5×10^{2}	0	0	0	0.026	6.0×10^{-3}
MS3	0.89	0.12	9.1	8.5×10^{3}	0.24	1.2×10^{15}	6.3×10^{12}	7.1	2.4×10^{3}	1.9×10^{2}	0.77	2.3×10^{15}	4.3×10^{14}	0.32	0.066
MS4	0.90	0.12	9.0	8.7×10^{3}	0.42	1.3×10^{15}	6.4×10^{12}	7.0	2.3×10^{3}	1.8×10^{2}	1.1	2.7×10^{15}	4.4×10^{14}	0.38	0.060
MF1	0.78	4.9	0	0	0	0	3.9×10^{14}	0	0	0	0	0	0	0	0
MF2	0.71	0.39	11.0	5.3×10^{3}	0	0	1.8×10^{13}	8.8	1.2×10^{4}	3.3×10^{2}	0	0	0	2.6×10^{-3}	7.6×10^{-4}
MF3	0.74	0.42	11.0	7.5×10^{3}	0.12	2.7×10^{15}	5.7×10^{13}	7.8	2.4×10^{4}	5.5×10^{2}	0.73	1.4×10^{16}	1.3×10^{15}	0.38	0.065
MF4	0.73	4.6	0	0	0.054	9.0×10^{15}	3.6×10^{14}	0	0	0	0.19	5.6×10^{16}	2.6×10^{15}	0.090	0.014
MF5	0.79	4.5	2.4	1.2×10^{4}	0.064	1.2×10^{16}	3.6×10^{14}	1.1	4.2×10^{4}	7.1×10^{2}	0.54	2.2×10^{16}	2.5×10^{15}	1.4	0.083
MF6	0.78	3.6	7.7	4.5×10^{4}	0.091	1.5×10^{16}	3.4×10^{14}	3.8	1.4×10^{4}	1.2×10^{3}	0.74	1.9×10^{16}	5.3×10^{15}	1.4	0.17
MF7	0.75	1.2	9.4	1.7×10^{4}	0.11	5.4×10^{15}	6.9×10^{13}	5.4	1.2×10^{4}	5.3×10^{2}	1.1	1.5×10^{16}	1.9×10^{15}	0.76	0.13
MF8	0.74	1.2	9.5	7.3×10^{3}	0.024	3.2×10^{15}	1.1×10^{14}	6.8	5.8×10^{4}	7.6×10^{2}	0.49	1.3×10^{16}	1.8×10^{15}	0.35	0.077

Note. — M_{IC} : the inner core mass at bounce in unit of $M_\odot$. ρ_c : the central density at bounce in 10^{14}g/cm^3. The ratios $|T/W|$ and $|E_m/W|$ are given in percentage. The angular velocity is presented in rad/s and the magnetic field is presented in G. The subscripts "b" and "fin" imply values at bounce and those at the end of simulation, respectively. The subscript "av" stands for the average value over the region with $\rho > \rho_c/1000$. E_{exp} : the explosion energy in 10^{51}erg. M_{ej} : the ejected mass in $M_\odot$.